RESTRAINED SHRINKAGE BEHAVIOR OF HEAT-CURED, HIGH EARLY-STRENGTH HIGH-PERFORMANCE CONCRETE (HES-HPC)

By

JONATHAN EAGELTON

A Thesis Submitted to the

Graduate School – New Brunswick

Rutgers, The State University of New Jersey

in partial fulfillment of the requirements

for the degree of

Master of Science

Graduate Program in Civil and Environmental Engineering

written under the direction of

Dr. Hani H. Nassif

and approved by

_____

_____

_____

New Brunswick, New Jersey

January 2014

ABSTRACT OF THE THESIS

Restrained Shrinkage Behavior of Heat-Cured, High Early-Strength High-Performance Concrete (HES-HPC)

by JONATHAN EAGELTON

Thesis Director:

Dr. Hani H. Nassif

For decades, High Performance Concrete has commonly been used in bridge decks due to its high strength and durability. Despite these properties, cracking in decks continues to be a challenge for bridge engineers. Cracking in bridge decks can lead to weaker structural members, increased damage during freeze-thaw cycles, and accelerated corrosion. These issues lead to more frequent maintenance as the deck needs to be replaced, which raises costs. Causes of cracking includes: harsh weather conditions during pour or curing, high shrinkage stresses, and extremely high live loads due to overweight truck traffic. There is some belief that freshly poured concrete will develop some stress as adjacent lanes are loaded with trucks. Since the concrete is still weak at this stage, it is believed that the strain caused by this stress generation may be large enough to cause cracking.

Because of this, the New Jersey Turnpike Authority (NJTA) has recently developed Supplementary Technical Specifications for a High Early Strength HPC (HES-HPC) to replace bridge decks during staged construction. Higher early age strength can

be achieved by increasing the rate of hydration, which can be accomplished with higher temperatures. Part of the specifications suggests the use of a heat blanket to keep the concrete at higher temperatures in the early hours to achieve a faster strength gain. Despite this proposition, heat blanket cured concrete has yet to be tested for restrained shrinkage using the ring test. Additionally, shrinkage reducing admixture has yet to be studied for HES-HPC, despite the possibility of its applicability.

The restrained shrinkage ring test is used to compare the cracking tendency of HPC, typical HES-HPC, and heat cured HES-HPC. Shrinkage reducing admixture is also studied to determine if it can be practically applied to HES-HPC. Results of the restrained shrinkage test are also correlated with the free shrinkage results. Crack development is monitored throughout the test and used for comparison.

ACKNOWLEDGEMENTS

I would like to thank Dr. Hani H. Nassif for his guidance and support during the completion of my undergraduate and graduate degrees. His support motivated me to apply for the Fellowship I never thought I would be awarded.

I would also like to thank Dr. Husam Najm and Dr. Hao Wang for being part of my thesis committee. They have provided me with great advice and have taught me so much.

I would like to thank my family for their constant support throughout my life.

I would like to thank Liat Kisos for her unwavering love and support. She has supported me in every aspect of my life for as long as I have known her.

I would like to thank Phil Darold, Zeeshan Ghanchi, Adi S. Abu-Obeidah, Clifford Chang, Miguel Beltran, and Michael Salvador for all the joy they have brought to work each and every day.

I would like to thank Dan Su and Peng Lou for all the help and advice they have provided me. Their knowledge and experience is astonishing.

I would like to thank Ken De Groh, Kyle Young, Yarissa Subervi, Dalexander Gonzalez, and David Fahim for all their help and kindness.

TABLE OF CONTENTS

LIST OF TABLES

LIST OF FIGURES

CHAPTER 1

INTRODUCTION

1.1 PROBLEM STATEMENT

High Performance Concrete (HPC) has been used in bridge decks for decades, due to its high strength and durability. Despite the high strength capabilities, deck cracking is still the most critical issue a bridge faces during its design life. Cracking can lead to weaker structural members, increase in damage during freeze-thaw cycles and, if the crack penetrates to the steel reinforcement, can lead to accelerated corrosion. Causes of cracking includes: harsh weather conditions during pour or curing, high restrained shrinkage strains reaching the cracking strain, and extremely high live loads due to overweight truck traffic. While harsh weather may only be avoided to a degree through proper scheduling, and overweight trucks may only be prevented as the technology for weight monitoring systems improves; early age strength and shrinkage are factors we have more control over. Concrete shrinkage cannot be prevented, but it may be reduced with proper curing and the use of appropriate materials.

In addition to high shrinkage strains, truck traffic in adjacent lanes during staged construction will also produce stresses in the freshly poured deck. Traffic cannot be stalled for long periods of time, so it is important for as many lanes as possible to be available for the morning and evening commutes. Early crack development is believed to be caused by truck traffic in the adjacent lanes during the first 24 hours after the pour.

Although the weight of the truck is not applied directly onto the new deck, some of the load will be distributed while the concrete is still weak. Thus, it is believed that higher early age strength can help prevent cracks from developing before the lane is open for traffic.

The New Jersey Turnpike Authority (NJTA) has recently developed Supplementary Technical Specifications for a High Early Strength HPC (HES-HPC) to replace bridge decks during staged construction. Higher early age strength is achieved by increasing the rate of hydration, with the use of set-accelerating admixture and higher curing temperatures. During the summer the high ambient temperatures are enough to produce the strength required, but during the fall, when ambient temperatures start falling, a heat blanket is recommended to help achieve the desired strength. With the methods used in the specifications, it is possible for the concrete to produce a strength of 1,200 psi in just 6 hours after casting. However, this is still a fairly new use of concrete, and the shrinkage/crack development still needs monitoring to understand the effectiveness of these mixes.

1.2 RESEARCH OBJECTIVE AND SCOPE

This study evaluates early age strength and long term shrinkage/cracking effects of HES-HPC mixes, as well as the variation in early age strength development. Mix proportions are based on the HES-HPC mix designs, as specified in the NJTA's Specifications. The study examines 14 mixes performed in the lab, including mixes classified as HPC and HES-HPC. For comparison, each mix performed in the lab contains samples which are cured under 2 different conditions: normal curing and 1 day

heat blanket curing. Heat blanket curing is followed by standard moist curing until day 14. Parameters examined in the study include: heat curing and normal curing, fly ash and slag, and Shrinkage Reducing Admixture (SRA).

1.3 THESIS ORGANIZATION

This thesis is composed of five chapters organized in the following manner:

Chapter 1 presents the problem statement, objective, and scope of the study.

Chapter 2 presents a literary review of the topic in question. The literature review provides a background on the types of shrinkage, and the restrained shrinkage ring test. This chapter provides the basis of design for the experimental program.

Chapter 3 explains the experimental methodology used in the study. This includes materials, mixing procedures, testing standards, and parameters.

Chapter 4 presents all test results, including free and restrained shrinkage, compressive and tensile strength, modulus of elasticity, as well as the correlation of Foil Strain Gages and Vibrating Wire Strain Gages.

Chapter 5 presents the conclusions drawn from the study, as well as a discussion for future research.

CHAPTER 2

LITERATURE REVIEW

2.1 INTRODUCTION

Volume change in concrete is an unavoidable phenomenon. When the concrete is restrained as is the case for most structures, cracking becomes likely due to high tensile stress development. Significantly wide and deep cracks can accelerate the corrosion of reinforcement, which will lead to a necessary repair in the structure. This is most notably a concern in bridge decks, which need repeated maintenance during the design life of the structure. Much has been studied on the shrinkage behavior of concrete, and what effects different materials may have on this behavior. It is clear concrete shrinkage and cracking cannot be prevented, but there have been great strides in crack mitigation techniques. A discussion of the causes of shrinkage, and previous studies on the topic, follows in the sections to follow.

2.2 TYPES OF SHRINKAGE

Concrete will shrink for various reasons over its lifespan. The total shrinkage is the summation of the individual causes of shrinkage. The degree and rate of shrinkage generally depends on the types of materials used, but also the method of curing used. Some types of shrinkage can be controlled to a point where the shrinkage is almost nonexistent, while others cannot be avoided but controlled to reduce the effects.

Shrinkage will lead to internal stresses developing if the concrete is restrained, which will lead to cracking if the shrinkage is not controlled. This makes shrinkage a major concern if the concrete experiences any loading before it finishes the intended curing length. The combination of low early strength, early loading, and high early age shrinkage can lead to extreme cracking problems. The various types of shrinkage and the known causes for them are discussed below.

2.2.1 Plastic Shrinkage

Plastic shrinkage occurs while the concrete is still fresh, prior to the hardening of the concrete. It is due to the rate of evaporation being greater than the rate of bleeding. The degree of plastic shrinkage depends on how high the rate of evaporation is, which mostly depends on the concrete's exposure to environmental factors. The types of environmental factors which can increase the rate of evaporation include: high temperatures, high wind speeds, and low relative humidity. Special care should be taken if these conditions exist where the concrete is poured. A study done by Tia et al. has shown that plastic shrinkage can be greatly reduced with wet burlap curing and covering with a plastic sheet shortly after the concrete is cast (2005). This eliminates some of the environmental factors that affect plastic shrinkage. Additionally, SRA has shown to reduce plastic shrinkage cracking (Lura et al., 2007).

2.2.2 Thermal Shrinkage

While the concrete hydrates, it experiences a noticeable increase in temperature, commonly known as the "heat of hydration". This increase in temperature is generally an indicator of the concrete's setting time, which will be followed by the concrete hardening and its temperature decreasing back to the environments temperature. The decrease to

reach the ambient temperature is when thermal shrinkage occurs. The development of temperature in the concrete will depend on its dimensions, geometry, thermal properties, the conditions at placement, and the environmental conditions (Emborg and Bernander, 1994). The specific heat and thermal diffusivity of concrete has been shown to decrease linearly as the degree of hydration increases (Schutter, 2002). Additionally, studies have shown that HPC typically has higher thermal shrinkage due to higher hydration heats, which becomes more of a concern with thicker slabs of concrete (Acker and Ulm, 2001). Thermal shrinkage is mostly unavoidable due to the heat of hydration occurring regardless of the ambient temperature, but there are methods to reducing it. Byard et al. reported that Granulated Blast-Furnace Slag, a common pozzolan found in HPC, has shown a delayed and reduced peak temperature rise during hydration, which leads to a reduction in thermal stress (2010). Furthermore, the ultimate value of thermal shrinkage is strongly dependent on the coefficient on thermal expansion, which is at a minimum when relative humidity is 100% (Kovler and Zhutovsky, 2006). This can be achieved through wet burlap curing.

2.2.3 Autogenous Shrinkage

Autogenous shrinkage is the volume change of cement pastes, mortar, or concrete during the early ages of hydration. During hydration, the cement particles create a very fine pore structure which later becomes drained of its water. Self-desiccation occurs when there is not enough water to submerge the surfaces of unhydrated particles. It has been noted that during very early ages, when the concrete is still a fluid, the volumetric changes are not a concern due to the lack of stress generation while the concrete is deforming plastically. Once it transitions into a visco-elastic solid, stresses develop due to

what is known as autogenous shrinkage (Lee et al., 2006). Determining the initiation of this transition marks the beginning on stress development caused by autogenous shrinkage, making it very important for researchers to determine the appropriate time to begin recording. It has been suggested that setting time is directly related to the start of autogenous shrinkage. The penetration test is a common method for determining setting times, but Lee et al. discovered it to be inaccurate due to its need to be performed on a mortar and not concrete (2004). However, since the heat of hydration is a good indicator of setting time, monitoring the temperature can help approximate the start of autogenous shrinkage.

2.2.4 Drying Shrinkage

Once the concrete is done curing, the water deep within the capillary pore system of the hardened concrete begins to evaporate. The loss of the water in the pore structure causes what is known as drying shrinkage. Drying starts at the surface and slowly migrates to the internal water locked in the pore space. The rate of drying shrinkage will depend on the amount of exposed surface area and the same factors that increase evaporation, while the amount of total drying shrinkage depends on the pore space in the concrete. This shrinkage can occur over a prolonged time, depending on the volume of concrete, exposed surface area and relative humidity in the environment. Drying shrinkage is the most significant contributor to total shrinkage and can also be the hardest to control, making it a critical problem that is commonly researched.

SRA has become a commonly used material to control drying shrinkage, though how effective it is still needs to be monitored. Bents et al. witnessed a significant reduction in the surface tension of mortars containing SRA, and without any effects on 28

day strength (2001). However, this has not been studied if this is the case for HES concrete samples under heat curing.

2.3 FACTORS CONTROLLING SHRINKAGE

Due to how critical cracking has become in concrete decks, many studies have been done to discover the causes of crack development. Since the strain development due to loading cannot be controlled, a reduction in shrinkage strains has been the focus for controlling cracking. Because of this, studies have focused on determining the factors which control shrinkage. The various materials and quantities used in the mix proportions have the most effects on shrinkage, but other factors include curing techniques and environmental factors.

2.3.1 Materials

Nassif, Najm, and Aktas suggested coarse aggregate content, and the coarse aggregate to fine aggregate ratio appears to affect the shrinkage the most (2007). The report proves mixes with a high CA content of 1850 lbs/yd^3 and CA/FA greater than 1.48 leads to a much lower cracking potential in the restrained shrinkage ring test. Larger coarse aggregate sizes and higher volumes creates a more rigid concrete, increasing its resistance to shrinkage. Different coarse aggregate types, such as limestone and quartz, are known for producing more shrinkage.

Various cementitious materials found in HPC are also known to have effects on shrinkage, including cement, Flyash, Silica Fume, and Granulated Blast-Furnace Slag. Flyash, Silica Fume, and Slag are commonly used for its reduction in cost and its improved durability. Over time, cement manufactures have created several cement types,

with different pore sizes and different chemical porperties. Finer cement particles typically hydrate much faster than larger particles, and also leads to a finer pore structure, leading to higher shrinkage strains. Many experimental programs have been done on the different cement types to determine how effective they are and what the negative effects each may have.

There appears to be a lot of conflicting reports on the effects Flyash has on drying shrinkage. Some reports have shown that the inclusion of high dosages of Flyash will actually reduce drying shrinkage. A report by Atis even suggests that a combination of high-volume Flyash with a low water-cementitious material ratio reduced the shrinkage by 30% (2003). Another study by Kayali et al. showed no significant difference when comparing OPC and HPC containing Flyash (1999). Termkahjornkit reported that a 25% replacement of Flyash lead to an increase in autogenous shrinkage, while a 50% replacement of Flyash lead to a significant decrease in autogenous shrinkage (2005). These three studies are just an example of the many conflicting opinions on the material.

Silica Fume is a commonly used material in HPC due to its ability to reduce porosity and permeability during the hydration of Portland cement. Silica Fume is used in small doses as it is a highly reactive material which increases the rate of hydration and increases autogenous shrinkage. Although it has shown to have not a significant effect on shrinkage, it has shown that higher percentages of Silica Fume lead to an increase in autogenous shrinkage while the drying shrinkage decreased (Mazloom et al., 2004). It should also be noted that higher percentages of Silica Fume require more super-plasticizer due to its effects on the slump.

Ground Granulated Blast Furnace Slag (GGBFS) is another material commonly used in HPC. Slag's effects on shrinkage is believed to be related to the curing procedure, with a longer moist curing time leading to smaller total shrinkage compared to concrete made with OPC. Slag's effects on shrinkage has some conflicting opinions, with some reporting lower shrinkage than concrete with only OPC (Li and Yao, 2001), and some reporting higher shrinkage (Lee et al., 2006). One thing most studies agree upon is the fact that the use of Slag typically has a greater 28 day strength and higher shrinkage compared to Flyash (Haque, 1996).

2.3.2 Other factors

Special care should be taken to ensure proper curing methods are being performed as improper methods are ineffective for not only developing high 28 day compressive strength, but also can lead to higher shrinkage strains. 14 day moist curing is by far known to be the best method for reducing shrinkage effects. Wet burlap curing is another commonly used method, but is also not nearly as effective as moist curing (Nassif and Suksawang, 2002). Long curing lengths are typically known to reduce ultimate shrinkage, due to the concrete's sensitivity at earlier ages. Additionally, concrete that is consolidated using a vibrating table has shown lower shrinkage strains than concrete that is consolidated using conventional rodding (Loser and Leemann, 2009).

Many researchers have studied the effects of different curing methods, including temperature and duration. One study performed by Nassif et al. focused on the compressive strength and modulus of elasticity resulting from different curing procedures (2004). The curing methods applied in this study were wet burlap, curing compound and air-dry curing. Wet burlap curing resulted in the highest compressive strength and

modulus of elasticity. Kim et al. performed a study to monitor compressive strength development of concrete by varying curing temperature and curing length at various ages (1998). Changes in temperature were performed gradually to reduce the risk of thermal damage. The study found that high temperatures at early ages leads to an increase in early age strength but has a decreased later age strength. Lower temperatures, on the other hand, decreased early age strength but had no effect on later age strength. Additionally, the authors discovered the maturity strength relationship has been inaccurately modelled due to the concrete's higher sensitivity to temperature at very early ages. Huo and Wong performed a study to monitor early age temperature gain, moisture loss, and shrinkage strains of concrete under different curing conditions (2006). The authors found curing compound to have a much higher temperature increase due to hydration, and also had higher ultimate shrinkage. Additionally, higher evaporation rates, found in shorter curing lengths, also lead to higher shrinkage strains. This leads one to believe that great care should be taken to ensure there is no excessive moisture loss while curing under higher temperatures.

Environmental factors will affect the shrinkage by affecting the curing conditions and by changing the rate of hydration. Higher ambient temperatures during curing, for example, will have a negative impact on the plastic shrinkage. It may also cause higher autogenous shrinkage during the setting of concrete, by increasing the rate of hydration. Higher ambient temperatures during the early ages of curing is also the cause for higher strength at early ages, hence the concern for HES-HPC. Relative Humidity (RH) also can have an effect on shrinkage. Low RH values will increase the rate at which concrete

dries, increasing drying shrinkage. Harsh weather such as high winds will also affect the plastic shrinkage.

2.4 RESTRAINED SHRINKAGE RING TEST

The restrained shrinkage ring test is the most widely used test method for determining crack potential under restrained conditions. It is commonly accepted for being cost effective and a simplistic method, although other methods include the flat panel test and the linear restrained shrinkage test. ASTM and AASHTO have each developed their own standards for testing restrained shrinkage. The differences in these test methods are mostly related to the geometry of the ring and are described in the sections to follow.

2.4.1 Development of Ring Test

The first ring test was modelled and performed between 1939 and 1942 by R. W. Carlson and T. J. Reading (1988). This marked the first use of a restrained shrinkage ring to test concrete's durability in the restrained condition. They tested in different environments to test how the concrete behaved by varying relative humidity. Over time it has become a much more common test, but it was not until 1998 that standards were proposed for the test. AASHTO proposed their ring test, "AASHTO PP34-98: Standard Practice for Estimating the Cracking Tendency of Concrete", as a provisional standard in 1998, and was later approved in 2006 to full standards. ASTM approved their ring test, "C 1581 - 04: Standard Test Method for Determining the Age at Cracking and Induced Tensile Stress Characteristics of Mortar and Concrete under Restrained Shrinkage", in 2004 and has since been updated in 2009.

2.4.2 ASTM Ring Test

Similarly to the AASHTO ring test, the purpose of ASTM's ring test is to provide a relative comparison of induced tensile stresses and cracking tendency between mix materials. It is noted that the test is not intended for determining age of cracking of mortar or concrete for a specific structure, configuration, or exposure. It is accepted that variations in materials, such as aggregate sources, aggregate gradation, cement type, cement content, water content, cementitious materials, and chemical admixtures, will have effects on the results of the test. Besides the signaling of a crack, tensile stress development also provides a basis for comparison.

The ASTM ring test calls for a concrete ring of 1.5 inch (38 mm) thickness and height of 6.0 ± 0.25 in. (150 ± 6 mm) to be cast. The inside of the concrete ring is restrained by a steel ring of 0.5 ± 0.05 in. (13 ± 1 mm) thickness, an outside diameter of 13.0 ± 0.12 in. (330 ± 3.3 mm), and height of 6.0 ± 0.25 in. (150 ± 6 mm). The setup configuration, with dimensions, is shown in Figure 4.1 (ASTM C 1581, 2009). The base, as well as the outer ring, of the mold is to be a non-absorptive and non-reactive material. The outer ring mold is coated with a release agent for when the ring is demolded. Bolts are used in order to prevent the steel or outer mold to move, and ensure the correct dimensions of the concrete ring are cast. The ring is stored in an environmentally controlled room with constant temperature of 23.0 ± 2.0 °C (73.5 ± 3.5 °F), and a relative humidity of 50 ± 4%. A minimum of two strain gauges are attached to the inside of the steel ring to monitor the strain development in the steel. The strain gages are applied at mid-height, and diametrically opposite, with the gages oriented to measure strain in the

circumferential direction. The strain gages are set to collect at an interval no greater than 30 minutes.

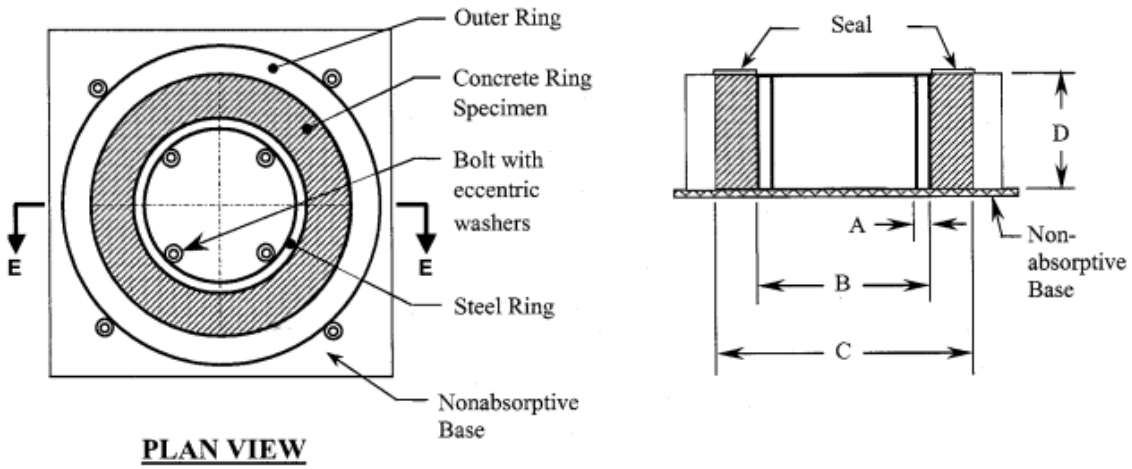

Figure Dimensions	SI Units	Inch-Pound Units
A	13 ± 1 mm	0.50 ± 0.05 in.
B	330 ± 3 mm	13.0 ± 0.12 in.
C	405 ± 3 mm	16.0 ± 0.12 in.
D	150 ± 6 mm	6.0 ± 0.25 in.

Figure 2.1 ASTM Ring Test Mold and Dimensions

The concrete is consolidated in two layers. While casting, the concrete is consolidate by using a vibrating table while simultaneously rodding through each layer 75 times. After consolidation, the proper methods are taken in order to achieve a flat surface on the top of the concrete ring. The ring is transferred to the environmental chamber within 10 minutes of casting and curing begins within 5 minutes of the first strain recording. Curing is performed by covering the ring with wet burlap and a polyethylene sheet. The mold is removed after 24 hours, and is covered with wet burlap and the polyethylene sheet for however long the desired curing process is. The top surface is sealed in order for drying to only take place circumferentially. The strain readings are monitored for sudden decreases in compressive strain, which indicates the

occurrence of cracking. The strain is monitored for a minimum of 28 days after the initiation of drying unless cracking has occurred prior to this. Age at cracking is recorded to the nearest 0.25 day, while the initial strain is recorded as the strain reading at the initiation of drying.

2.4.3 AASHTO Ring Test

Like the ASTM test, the AASHTO ring test is used to determine the effects of concrete variations on cracking tendency. Variations include aggregate source and gradation, cement type, cement content, water content, and mineral admixtures. It is noted that the test is helpful in determining the relative likelihood of early age cracking of concrete mixes, with actual cracking depending on bridge type, degree of restraint, construction and curing methods, and environmental factors. Time-to-cracking is measured as the time when an abrupt drop in strain is seen in the steel ring.

The main difference between the ASTM and AASHTO test is the dimensions of the ring. The steel ring has a wall thickness of 1/2 in. ± 1/64 in. (12.7 mm ± 0.4 mm), an outside diameter of 12 in. (305 mm), and a height of 6 in. (152 mm). The outside and inside of the steel much be machined smooth, round and polished. The forms are to be nonabsorbent and the top surface is wet cured using wet burlap and covered with plastic. During the testing, the samples are to be stored in a controlled-environment room with a constant air temperature of 73.4°F ± 3°F (21°C ±1.7°C), and relative humidity of 50 ± 4%.

Previous to pouring the concrete, the steel ring is coated with a release agent. The concrete is consolidated in 3 layers, and rodded 75 times per layer. External and internal vibration is not recommended, but it is not restricted. When finished, a flat top surface is

made, the strain gages are connected to the DAS, and the ring is covered with wet burlap and plastic once the concrete is hardened enough to resist the indentation of the burlap. The forms are removed after 24 hours ± 1 hour, then the top and bottom surfaces are coated with silicone caulk and sealed with plastic or rubber. The strains in the rings are to be monitored every 30 minutes. A strain decrease of more than 30 microstrains in at least one gauge usually indicates cracking.

2.5 PREVIOUS STUDIES

As previously stated, Carlson and Reading conducted the first concrete ring test in 1939 in order to compare the cracking behavior of mixes. The objective of the study was applied to concrete mixes to be used in restrained walls. The study focused on the cracking effects of changing relative humidities. This ring was of 1 in. (25 mm) thickness and a 1 in. thick steel ring, with an outer diameter of 7 in. (175 mm). Once the concrete finished curing, the top and bottom surfaces were sealed to prevent moisture escaping these surfaces. Free shrinkage samples were also prepared to correlate with the restrained shrinkage results. This is the first instance of the ring test being used for correlation with free shrinkage testing. Results showed that lower relative humidities resulted in higher stress development, which resulted in an earlier cracking age.

The restrained shrinkage test performed by Carlson and Reading was uncommon at the time it was initially reported. It was not until the late 90s that the test became commonly accepted by other researchers, prompting standardized testing methods to be developed. Due to the lack of a standardized testing method prior to this, different ring geometries and methods were used between researchers. Banthia et al. described this lack

of a standard testing method for restrained shrinkage, though discussed the ring test as one of the techniques to be developed by the time of his study in 1993. In addition to the ring test, the “doubly restrained plate specimens” and the “uniaxial tests” is mentioned as a restrained shrinkage test method, but is stated that the doubly restrained test is dependent on specimen geometry and the uniaxial test is prone to errors.

In 1997, K. J. Folliard and N. S. Berke performed the ring test to determine the shrinkage properties of HPC containing SRA. This test was modified from the method used by Carlson and Reading. For testing, a concrete ring of 2 in. (50 mm) thickness and 6 in. (150 mm) height was cast around a steel pipe with an outside diameter of 12 in. (300 mm) and a 1 in. (25 mm) thickness. Samples were moist-cured at a temperature of 68°F (20°C) and 50% RH for 24 hours before being sealed on the top surface with polyurethane. Free shrinkage prisms were also cast and cured under the same conditions to correlate free and restrained shrinkage results. Four different mix designs were used to study the differences between Portland Cement concrete and Silica Fume, and compare the results of mixes containing SRA with the results of mixes without SRA. The results of the study show that for silica fume based mixes the inclusion of SRA lead to a 52% reduction in 28 day drying free shrinkage and a 43% reduction in 120 day drying free shrinkage. The benefits of SRA were not as significant for regular Portland Cement concrete, but still high with a 35% and 29% reduction at 28 days and 120 days, respectively. It is suggested by the authors that SRA’s positive effects on shrinkage become even more apparent when a longer curing cycle is used. For the Portland Cement control mix, the average time to the first crack was 44 days. When SRA was added to the mix proportions, the rings showed no signs of cracking within the 120 day testing period.

For the Silica Fume based mix, the average time of cracking was 38 days without SRA and 95 days with SRA. The authors concluded that including SRA lead to a decrease in strength but also a more significant decrease in free and restrained shrinkage.

A similar study was performed in 1999 by Zonghin et al. to discover the restrained shrinkage effects by varying several material quantities. The materials used as the parameters for the study include, ground granulated blast furnace Slag, Flyash, Silica Fume, and Calcium Nitrite Inhibitor. A concrete ring of 1-3/8 inch (35mm) thickness and 5-1/2 inch (140 mm) height was cast around a 1 in. (25 mm) thick steel ring with a 12 in. (305 mm) outer diameter. After 24 hours, the outer mold is removed and the top surface of the ring is sealed with an epoxy resin. A free shrinkage ring was also made, with the inner circumferential surface being coated with epoxy resin as well. Samples were moist-cured with a 100% RH for 4 days at a temperature of 68°F (20°C). This was followed by drying in an environment with a 40% RH and 68°F (20°C). The free shrinkage ring contained five brass studs embedded in the top surface of the ring and measured with an extensometer every 24 hours for 10 weeks. The study found that an increase in Silica Fume, Flyash and Calcium Nitrite Inhibitor, lead to an increase in observed crack width. Interestingly, a Slag replacement of 50% showed an increase of over 100% in crack width but did not show any increase in free shrinkage strain. This indicated that free shrinkage strain does not always correlate well with the restrained shrinkage ring test, though this may also be an error with the method of testing.

Once AASHTO developed their provisional standards, the restrained shrinkage ring test has become more standardized, with there no longer being significant differences in the ring's geometry and curing methods. In 2003, Hossain et al. questioned

the provisional standard for its' limited ability to provide information on residual stress development. Despite the existence of the provisional standard provided by AASHTO, Hossain et al. used different dimensions of the ring and used various steel ring dimensions to determine the role of ring wall thickness (degree of restraint). All concrete rings in the study have a 3 in. (75 mm) thickness, and height of 3 in. (75 mm). The steel rings all had the same outer diameter of 12 in. (300 mm) but had wall thicknesses of 1/8 in. (3.1 mm), 3/8 in. (9.5 mm), and 3/4 in. (19 mm). Four strain gages were connected at mid-height of the inside of the steel ring. The circumferential surface of the specimen was sealed with two layers of aluminum tape after demolding at 24 hours. The specimen was then cured at a RH of 50% and a temperature of 73°F (23°C). Free shrinkage prisms were also cast according to ASTM C157 for correlation. The authors developed a model to calculate stresses in the restrained-ring specimens as an attempt to make the test more quantitative. The equation for the maximum tensile stress in the concrete ring under pressure is shown as:

$$\sigma_{Actual-Max}(t) = \varepsilon_{Steel}(t) * E_S * C_{1R} * C_{2R}$$

where,

$\sigma_{Actual-Max}(t)$ = maximum residual stress at time t,

$\varepsilon_{Steel}(t)$ = average steel strain at time t,

E_S = elastic modulus of steel, and

C_{1R} and C_{2R} = two constants that depend on the geometry of the ring and the steel material properties.

The authors concluded that this equation achieves its' purpose by making the ring test more quantitative. A thicker steel ring, which is equivalent to a higher degree of restraint,

showed a lower stress-strength ratio than lighter steel rings. Based on the results of the study, it is clear that differences in bridge geometry and degree of restraint will affect the time-to-cracking, but the ring test itself still provides information on trends, which is expected to be the same.

CHAPTER 3

EXPERIMENTAL SETUP

3.1 INTRODUCTION

In this experimental setup, mix designs were chosen based on the New Jersey Turnpike Authority's (NJTA's) recently developed Supplementary Technical Specifications for High Early Strength HPC (HES-HPC). Both Slag and Flyash based mixes are tested for comparison. All mixes contain a w/b ratio of .33, a total cementitious amount of 700 lbs/yd^3 and a 5% silica fume replacement. The methods used in this study were performed to compare free and restrained shrinkage, early age strength, and the short and long term effects of both heat curing, and shrinkage reducing admixture.

Material properties and proportions are discussed in greater detail below, as well as the procedures for sample collection and curing. Furthermore, all testing methods performed in this study for fresh and hardened concrete are described. The AASHTO ring test and the free shrinkage test are the most critical tests for this experimental program. These two tests are used to show the cracking potential of each mix and how the different methods affect the results of these tests.

3.2 MATERIAL PROPERTIES

The raw materials used in this study are: Type I Portland cement, Granulated Blast-Furnace Slag (GBFS), Silica Fume, Flyash, Coarse and Fine aggregates, and chemical admixtures. All chemical admixtures used are supplied by W.R. Grace, and includes Air Entraining Agent (AEA), High Range Water Reducer (HRWR), Set-Accelerating Admixture (SAA), and Shrinkage Reducing Admixture (SRA). The material types and suppliers are provided in Table 3.1.

Table 3.1 Material Properties and Suppliers

Material	Type	Supplier
Portland Cement	Type I	Essroc
Slag	Grade 100 GBFS	Holcim
Flyash	Type F	STI
Coarse Aggregate	Fanwood #57	Clayton
Fine Aggregate	Concrete Sand	Clayton
AEA	Daravair 1000	W.R. Grace
HRWR	ADVA Flex	W.R. Grace
SAA	Daraset 400	W.R. Grace
SRA	Eclipse 4500	W.R. Grace

The coarse aggregate has a maximum diameter of ¾ inches and was collected from the same location for all mixes, as well as the fine aggregate, to minimize possible errors. The moisture content of both aggregates are tested prior to mixing to ensure every mix has the intended w/c. HRWR doses varied to keep similar slumps between mixes. Also, HRWR has a slight retarding effect and the doses had to be limited to prevent it from affecting the early age strength.

3.3 MIX PROPORTIONS

A total of 6 mix designs were used for this study. Each mix design was performed 3 times, with the exception of the HPC-control mixes, for the purpose of showing variability in early age results, and covering every test required. There are a total of three groups of mix designs; the names and the description of each appear in Table 3.2. Both Flyash and Slag based mixes are performed in each group for comparison as well. The HES mix designs are based off of the NJTA's technical specifications for HES concrete, while the SRA mix designs are just altered to include SRA. The HPC mix designs are taken from previous experience.

Table 3.2 Mix Group Definitions

Group	Mix Names		Definition
G1 HPC/Control	G1-HPC-SL	G1-HPC-FA	Slag and Flayash based HPC, respectively
G2 HES	G2-HES-SL	G2-HES-FA	Slag and Flayash based HES Concrete, respectively
G3 HES-SRA	G3-SRA-SL	G3-SRA-FA	Slag and Flayash based HES-SRA Concrete, respectively

All abbreviations used for mix designs are provided in Table 3.3.

Table 3.3 Mix Design Abbreviations

Abbreviation	Definition
G1	Group 1 mixes
G2	Group 2 mixes
G3	Group 3 mixes
HPC	High Performance Concrete
HES	High Early Strength Concrete

SRA	Shrinkage Reducing Admixture
SL	Slag
FA	Flyash

Table 3.4 below provides the mix proportions for the Group 1 mixes. The Group 1 mixes are designed to be typical HPC mixes, and will not be heat cured or contain SAA. Both mixes contain a total cementitious content of 700 lb/yd^3, but contain a pozzolan replacement of 15% of Slag and 20% of Flyash. Dosages of HRWR are adjusted separately for each mix to achieve the target slump. Like most typical HPC mixes, there is a large course aggregate content of over 1800 lb/yd^3. Additionally, a low w/c of 0.33 is used for faster strength development. Air Entraining Admixture (AEA), a commonly used admixture in HPC, is also used to achieve the appropriate air content.

Table 3.4 Group 1 Mix Proportions

Material (lb/yd^3)	**G1-HPC-SL**	**G1-HPC-FA**
Portland Cement, Type I	570	535
Silica Fume	25 (3.6%)	25 (3.6%)
Slag	105 (15.0%)	-
Flyash	-	140 (20.0%)
Total Cementitious	700	700
Course Aggregate	1850	1820
Fine Aggregate	1230	1200
Water	231	235
w/c	0.33	0.33
AEA (oz/cwt)	2.0	2.0
HRWR (oz/cwt)	11.4	6.0
SAA (oz/cwt)	-	-
SRA (gal/yd^3)	-	-

Table 3.5 below provides the mix proportions for the Group 2 mixes. They consist of the HES mix designs, as specified by the NJTA's technical specifications. As previously stated, each mix was performed three times, so HRWR dosages varied slightly to achieve similar slumps. They contain high dosages of accelerator, at 50 oz/cwt, with the purpose of allowing the concrete to have a significantly higher rate of hydration. The w/c ratio is at the low value of 0.33, as it is also known that high w/c ratios cause a lower rate of hydration. Both Flyash and Slag mixes are performed within this group to show the differences in early and later age properties.

Table 3.5 Group 2 Mix Proportions

Material (lb/yd^3)	G2-HES-SL	G2-HES-FA
Portland Cement, Type I	570	535
Silica Fume	25 (3.6%)	25 (3.6%)
Slag	105 (15%)	-
Flyash	-	140 (20%)
Total Cementitious	700	700
Course Aggregate	1850	1820
Fine Aggregate	1225	1210
Water	230	231
w/c	0.33	0.33
AEA (oz/cwt)	1.2	1.5
HRWR (oz/cwt)	6.0-9.0	6.0-9.0
SAA (oz/cwt)	50	50
SRA (gal/yd^3)	-	-

Table 3.6 below provides the mix proportions for the Group 3 mixes. These mixes contain the identical mix proportions to the Group 2 mixes, but with the inclusion of SRA. The purpose of this group is to determine if SRA is a viable option for mitigating the shrinkage and cracking effects normally found on accelerated curing concrete. It can also help determine if it is plausible to include SRA in HES mixes, or if the retarding effect of SRA prevents it from gaining strength fast enough.

Table 3.6 Group 3 Mix Proportions

Material (lb/yd^3)	G3-SRA-SL	G3-SRA-FA
Portland Cement, Type I	570	535
Silica Fume	25 (3.6%)	25 (3.6%)
Slag	105 (15%)	-
Flyash	-	140 (20%)
Total Cementitious	700	700
Course Aggregate	1850	1820
Fine Aggregate	1225	1210
Water	230	231
w/c	0.33	0.33
AEA (oz/cwt)	1.2	1.5
HRWR (oz/cwt)	6.0-9.0	6.0-9.0
SAA (oz/cwt)	50	50
SRA (gal/yd^3)	0.5	0.5

3.4 MIXING AND FRESH CONCETE SAMPLING

In the following sections, the mixing procedure, fresh concrete tests, and sampling procedure are explained. All tests are performed according to the relevant ASTM standards, which is listed within the appropriate section. Immediately after mixing, the

slump and air content tests are performed, followed by the concrete sampling and the start of curing. It is important for all samples to be consolidated and cured in the same manner between mixes, to reduce any potential errors.

3.4.1 Mixing (ASTM C-192)

The mixing procedure is performed in accordance to ASTM C-192. First, the coarse and fine aggregate is added to the mixer, and the mixer is turned on briefly to uniformly mix the aggregates. Then, 1/3 of the water and all of the Air Entraining Agent is added, with the mixer being on for 30 seconds. This is followed by the addition of all cementitious materials and the remaining water. The mixer is turned on for a minimum of 3 minutes, and stopped at 1 minute intervals to briefly move any wet concrete stuck to the sides of the mixer. This is followed by a waiting period of three minutes, to let the concrete hydrate. This is then followed by the addition of any additional admixtures still to be added (accelerator and HRWR), followed by mixing for one to two minutes. This is then followed by the slump and air content tests. If the results are adequate, the sampling process can begin. If the slump is too low, additional HRWR can be added and mixed at this time. Figure 3.1 shows the concrete mixer used.

Figure 3.1 Concrete Mixer

3.4.2 Standard Test Method for Slump (ASTM C-143-12)

The slump test is performed with fresh concrete immediately after the mixing procedure in accordance with ASTM C-143-12. The slump of the concrete indicates the workability of the fresh concrete. The slump will also indicate, to some degree, how long the concrete will take to harden, which will also indicate how quickly the concrete will gain strength. For the purpose of this study, the target slump range is 2 to 4 inches, to ensure a quick setting concrete with high early strength gain. In practice, a higher slump is preferred so the concrete is easy to work with and will not begin to set before the pour is complete.

Once the mix is complete, the slump cone is filled in layers one-third of the height of the cone. After each layer of the cone is filled, the concrete is rodded 25 times throughout its depth with a steel rod. Once the slump cone is filled and rodded, excess

concrete is leveled off with a tamping rod or trowel. The slump cone is slowly lifted up to allow the concrete to “slump”. The cone is placed next to the concrete and the difference in height of the slump cone and the slumped concrete cone is measured. If the concrete shows any sign of shear or a “falling over”, the test is inaccurate and needs to be repeated. The slump measurement is depicted in Figure 3.2.

Figure 3.2 Measuring Slump

3.4.3 Standard Test Method for Air Content (ASTM C-231-10)

The air content test is performed in accordance to ASTM C-231 using a Type B Pressuremeter, shown in Figure 3.3. Prior to the start of the test, the pressuremeter is rinsed out with water. Once rinsed out, the container is filled in one-third layers, rodding 25 times throughout the depth of the most recently poured section. After rodding each section, a rubber mallet is used to tap on the sides of the container approximately 10 to 15 times, in order for the concrete to properly consolidate. The top layer of concrete is then levelled off with a rod or plate and the sides of the container are cleaned with a wet sponge. The top of the pressuremeter is then place carefully on the top of the container

and is sealed tightly. The air valve is closed tightly, and the two petcocks are left open. Clean water is poured into the petcocks completely so water comes out of both sides, and then they are closed. The pressuremeter can then be pumped until the reading on the dial reaches zero. This gage is tapped lightly to ensure there is an accurate reading. The air release lever can then be pushed to measure the air content. After the test is finished, the pressure can be released, the top of the container is removed and then the pressuremeter can be cleaned.

Figure 3.3 Type B Pressuremeter

3.4.4 Sampling and Consolidation of Specimen

All samples, including cylinder, free shrinkage molds, and rings, are consolidated using a vibrating table, pictured in Figure 3.4. Enough 4 x 8 inch cylinders are made to

cover all tests for each of the curing conditions, which will be discussed in the next section. All tests performed on the cylinders are discussed in detail in the sections to follow. Each mold is filled and consolidated for each half of the filled molds. A vibrating table is used because it is believed to be the best way of consolidating the concrete, limiting any significant voids in the concrete. The free shrinkage prisms are leveled off and then wrapped with plastic sheets to keep moisture in during the first 24 hours of the concrete's curing. Two free shrinkage samples are used for each curing type in order to take the average of the samples and verify results. The ring molds consist of an inner steel ring and Sonotube, which is removed after 24 hours. The free shrinkage and restrained shrinkage tests are discussed in detail in the sections to follow.

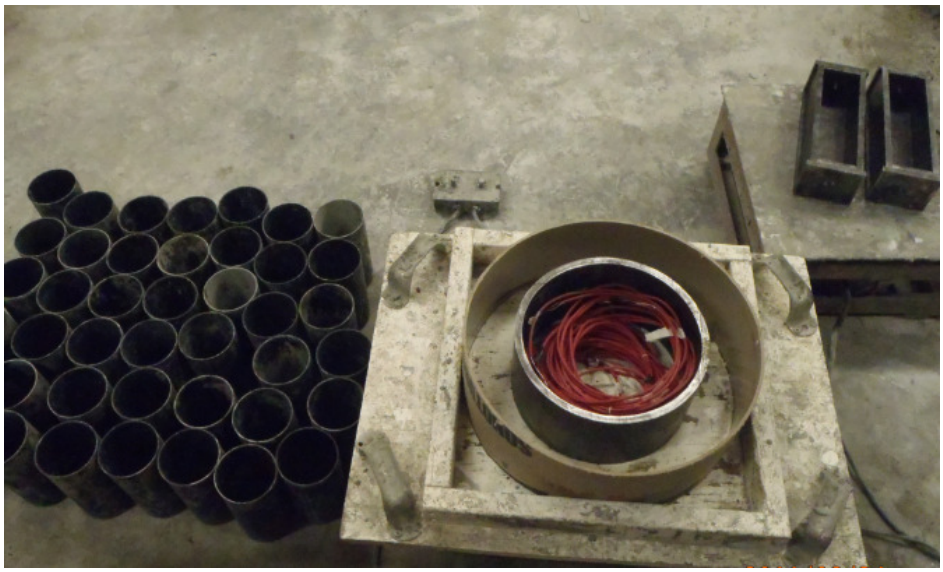

Figure 3.4 Sample Molds and Vibrating Tables

3.4.5 Curing Procedures

Two curing conditions exist for each mix: normal curing and 1 day heat blanket curing. 1 day heat blanket curing is used to achieve higher strength within the first 24 hours, and is monitored for what other effects it may have on the concrete. Samples under

the heat blanket are also covered with wet burlap, due to the risk of significant moisture loss in the concrete from the high temperature. After heat blanket curing is complete, the samples are cured in the same way as the normal curing samples, which are moist cured until 14 days. The heat blanket chamber is shown in Figure 3.5. After the 24 hour curing period, the cylinders are kept in a moist curing room, filled with humidifiers to achieve a relative humidity of 100%. The heat cured samples are loosely covered to allow them to cool gradually to room temperature. Although there is not an extreme temperature difference, it is important to rule out the possibility of the samples generating significant stresses caused by thermal shock. The free shrinkage samples and rings are wet burlap cured and covered with polyethylene sheets, while they stay in an environmental chamber with a constant temperature of 74°F and 50 ± 4% relative humidity. Figure 3.6 shows how the ring is covered, while Figure 3.7 shows the curing room and the environmental chamber. The burlap is monitored and changed daily to ensure the samples stay moist until 14 days has passed. The burlap is removed after 14 days, and the cylinders in the moist curing room are also moved to the environmental chamber.

Figure 3.5 Heat Blanket Chamber

Figure 3.6 Wet Burlap Curing for AASHTO Ring

Figure 3.7 Environmental Chamber (left) and Moist Curing Room (right)

3.5 TESTING PROCEDURES

The sections to follow contain detailed information on all laboratory tests performed for this study. The tests include compressive strength, tensile strength, modulus of elasticity, and free and restrained shrinkage. The ASTM standards followed, as well as any additional equipment required are listed in each section. Additional recommendations for early age compressive strength testing are stated based on the experience gained from this study.

3.5.1 Compressive Strength of Cylindrical Concrete Specimens (ASTM C-39-12)

A minimum of two 4 x 8 in. cylindrical concrete specimens are tested in accordance with ASTM C-39-12 using the Forney 1-Million Pound Compression Machine as shown if Figure 3.8. A third specimen is tested if there is a significant difference in the two compressive strengths. Any obvious outlier is ignored in calculating the average compressive strength. Tests are performed at 1, 3, 14, and 28 days, as well as the early age tests at 6, 7, 8, and 12 hours. For consistency, all cylinders use high strength sulfur capping for all testing dates. As ASTM does not specify any constraints for testing this early, recommendations are made for the appropriate methods for testing early age compressive strength. Early age strength testing should be capped with sulfur and tested within five minutes of the specified testing time. This is especially important for the heat curing specimens, which have a significantly increased rate of strength gain. Special care is taken to ensure the testing times are well recorded to reduce misleading results. The loading is set to a constant rate of 4,000 pounds per 9 seconds.

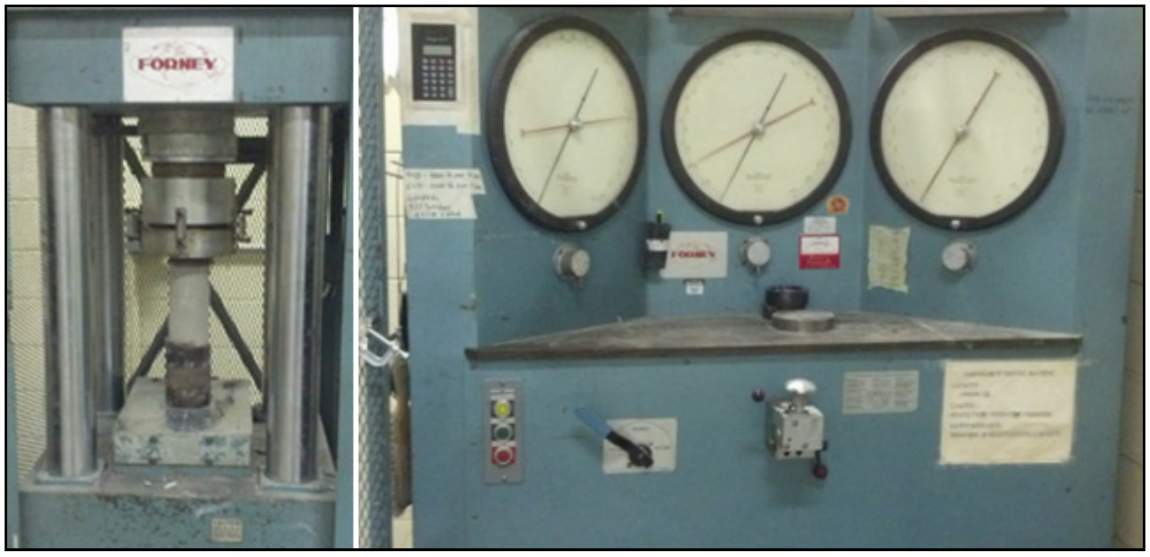

Figure 3.8 Forney 1-Million Pound Compression Machine and Cylindrical Concrete Specimen

3.5.2 Standard Test Method for Splitting Tensile Strength of Cylindrical Concrete Specimens (ASTM C-496-12)

Testing of the Splitting Tensile Strength is done in accordance with ASTM C-496-11 using the Tinius Olsen Compression Machine. A minimum of two 4 x 8 in. cylinders are tested with a third being tested if the difference is significant. As with the Compressive Strength testing, any obvious outlier is ignored in calculating the average. The specimens are loaded at a constant rate of 100 pounds per second. Two bearing strips are used with 1/8 in. thick plywood, with 1 in. width and a length that is at least as long as the cylinder length. They are placed between the specimen and both the upper and lower bearing blocks of the testing machine. Figure 3.9 shows the setup of the splitting tensile strength test.

Figure 3.9 Tinius Olsen Compression Machine with loaded cylinder

3.5.3 Standard Test Method for Static Modulus of Elasticity (ASTM C-469-10)

The Modulus of Elasticity is measured in accordance with ASTM C-469-10. A minimum of two 4 x 8 in. cylindrical specimen with high strength sulfur capping are required to be loaded three times. A compressometer is attached to the cylinders to measure the change in length for the specified loading cycle. A cylinder with compressometer attached is shown in Figure 3.10. The first loading is done without any measurements, in order for the "seating of the gages". Measurements are taken during the two subsequent loadings at every 2,000 pounds if the maximum loading is less than 20,000 pounds or at every 4,000 pounds if the maximum loading is at least 20,000 pounds. The cylinders are loaded up to 40% of the ultimate compressive strength. A third cylinder is tested if the Modulus of Elasticity of two cylinders have a significant difference. The Forney 1-Million Pound Compression Machine is used for this test.

Figure 3.10 Compressometer Attached to Cylinder

3.5.4 Drying Free Shrinkage Test (ASTM C-157-08)

The Free Shrinkage test is done in accordance with ASTM C-157-08 by using 3x3x11-1/4 in. concrete prisms, which are cast with a gage stud at their ends. Two prisms are used to ensure the results of one prism are an accurate depiction of the drying shrinkage for the specified concrete mix design. The length of each prism is monitored with a length comparator with the ability to measure to the nearest .0001 inches, shown in Figure 3.11. A reference bar is used to zero the comparator. The length of each prism is measured from the end of curing, 14 days from mixing, up to 56 days. The results are plotted in the form of strain over days past. Multiple measurements are taken on each testing date to confirm the correct measurement was taken and to limit human error. The samples are kept in a room with a controlled temperature and humidity so the effects of

thermal shrinkage are nonexistent. Samples are also kept on shelves with enough space to allow sufficient exposure for evenly distributed drying.

Figure 3.11 Length Comparator with Reference Bar and Prism

3.5.5 Restrained Shrinkage Ring Test

The restrained shrinkage test is performed in accordance with AASHTO PP34, and modified to include VWSGs. Concrete is cast around a steel ring with an outer diameter of 12 inches and a thickness of ½ an inch. An 18 inch Sonotube is used for the mold, creating a 3 inch thick concrete ring. As the concrete shrinks, a compressive stress is applied to the steel ring, which is transferred to the concrete as a tensile stress. If the tensile stress in the concrete exceeds the allowable tensile stress, the concrete cracks. Two types of strain gages are used during the test to monitor the strain readings in the steel and concrete rings. Four Foil Strain Gages (FSGs) are attached to the steel ring, while six Vibrating Wire Strain Gages (VWSGs) are embedded within the concrete ring. The gages can indicate a crack forming based on a release of tension in the steel (FSG) or

a high tensile strain in the concrete (VWSG). How the gages are attached and the method of collecting data is described in detail in the sections to follow. Furthermore, the ring is crack mapped at various ages with a digital microscope. Crack lengths and widths are measured and monitored for elongation. The digital microscope is shown in Figure 3.12.

Figure 3.12 Digital Microscope Setup with Laptop Showing Crack

3.5.5.1 Foil Strain Gauge (FSG) Instrumentation for Ring Test

The foil strain gauges, shown in Figure 3.13, are manufactured and supplied by Vishay Micro-Measurements. The gauges used are full bridge, 120 ohm resistance, with a 0.6% tolerance. They are attached to the inside of the steel ring on 4 sides, equally spaced apart. Although AASHTO PP34 requires a minimum of two strain gauges, four gauges was chosen for two purposes. Four gauges also allows for a better approximation of the correct location of cracking. The purposes are: more gauges can pinpoint when and where a crack occurs more accurately, and if one or two sensors fail for any reason the ring still has enough sensors to be in accordance with AASHTO PP34. The ring is first sanded and cleaned with an industrial cleaner. The gauge is attached with sensor adhesive and sensor tape. The gauge is covered with epoxy to protect the sensor, and the other end of the wire is connected to the data acquisition system (DAS).

Figure 3.13 Foil Strain Gauges

3.5.5.2 Vibrating Wire Strain Gauge (VWSG) Instrumentation for Ring Test

The vibrating wire strain gauges, shown in Figure 3.14, are manufactured and supplied by Geokon. The Model 4000 strain gauge contains a steel wire inside, which vibrates differently under as the sensors mounts move. The strain reading depends on the frequency at which the steel wire vibrates, which can read compression or tension. The gauges are used to monitor the strain in the concrete. Six gauges are connected in a hexagonal shape, with 3 inch long bolts being used for the embedment of the sensors into the concrete ring, as shown in the figure below. The resonant frequency is measured in each VWSG using an electromagnetic coil connected to the DAS through a connecting cable.

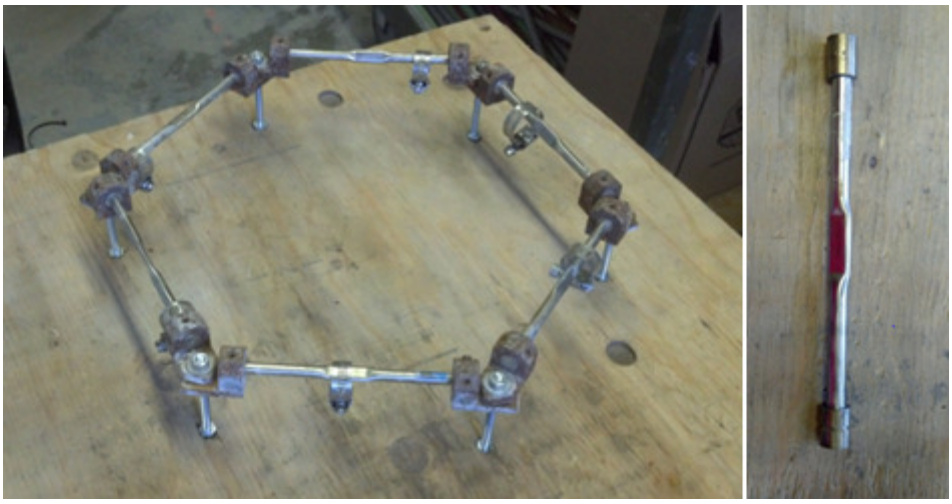

Figure 3.14 Vibrating Wire Strain Gauge Setup

3.5.5.3 Data Acquisition System (DAS) for Restrained Shrinkage Ring Test

Strain and temperature readings for the restrained shrinkage test are collected via a data acquisition system (DAS) manufactured by Campbell Scientific, Inc. The DAS is set to record readings every two minutes, and is collected from a computer connected to the system. The DAS is depicted in Figure 3.15.

Strain readings are monitored daily for any significant changes that would signal cracking, and the results are plotted periodically. The cracking strain is also plotted to help determine location and time of cracking. The cracking strain is determined from the splitting tensile strength and the modulus of elasticity. The equation is as follows,

$$\varepsilon_t = \frac{f_t}{E}$$

Where, ε_t is the cracking strain, E is the modulus of elasticity, and f_t is the splitting tensile strength. The data is collected for a period of 56 days. When the final plot is constructed, the results are compared with the results of the crack maps to match up the day of cracking and the location of cracking.

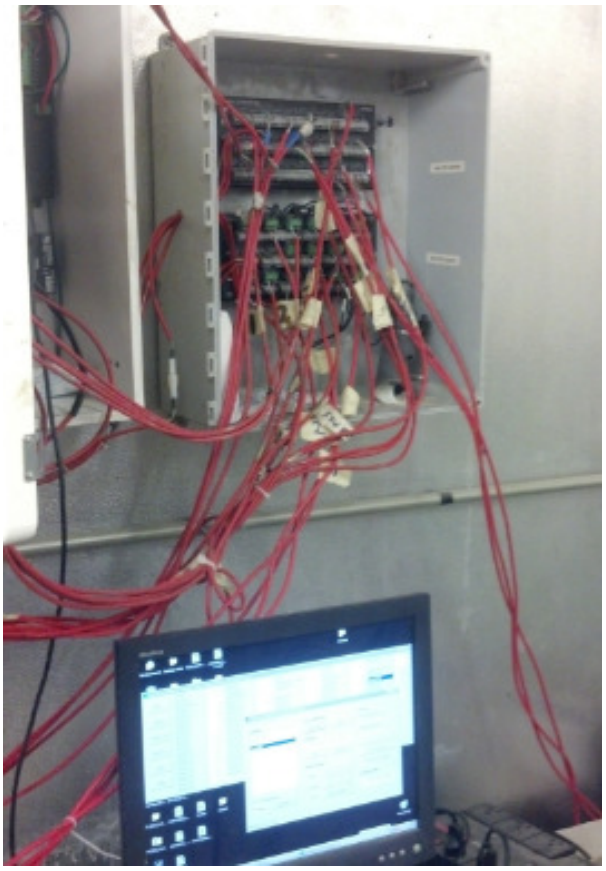

Figure 3.15 Data Acquisition System (DAS)

CHAPTER 4

TESTING RESULTS

4.1 INTRODUCTION

This chapter presents all results performed on all the mixes performed in this study. The testing results include mechanical properties, such as compressive strength, tensile strength and modulus of elasticity. Results for free and restrained shrinkage will also be a focal point in the sections to follow. Results will be presented according to what group they are in so they can be compared between themselves, and then the mixes within each group will be compared to other groups. As previously stated, each mix design was performed with three different batches to cover all tests needed and to show the variability of HES concrete.

4.2 FRESH CONCRETE RESULTS

As previously stated, immediately after mixing, the concrete is checked for slump and air content. Some of the mixes required additional HRWR to reach an adequate slump, which is the reason for the varying dosages in each mix. For the purpose of this study, low slumps of 2 to 4 inches were the target, as high slumps delayed the concrete strength gain. When applying this to bridge decks, higher slumps are recommended as more time is required for the pour, and there should not be a loss of early strength gain due to the

cement truck mixes a larger batch for a much longer period of time. The results for slump and air are provided in Table 4.1.

Table 4.1 Slump and Air Content Results

Mix Name	Batch	Slump (in)	Air Content (%)
G1-HPC-SL	-	4.25	2.60
G1-HPC-FA	-	4.00	3.25
G2-HES-SL	A	4.00	2.50
	B	3.00	2.50
	C	3.00	2.75
G2-HES-FA	A	3.50	3.00
	B	3.00	3.60
	C	2.75	3.40
G3-SRA-SL	A	2.50	3.00
	B	2.50	3.20
	C	4.00	3.00
G3-SRA-FA	A	4.00	2.75
	B	3.00	2.50
	C	2.50	2.60

4.3 MECHANICAL PROPERTIES

4.3.1 Early Age Compressive Strength

Due to the importance of early age strength to this study, this section is separated to compare the results between Flyash and Slag mixes, and mixes with and without SRA. Each table presents the results of 3 batches from the same mix design, and includes the average and coefficient of variation from the batches. Group 1 mixes are not include, as they are typical HPC mix designs, and did not include an early age testing prior to 24 hours. The results of the 24 hour test for Group 1 mixes will be included in the discussion for reference. Compressive strength results are presented in psi, and are shown as the

average of two or three tests. All tests are within the acceptable variation limits. The results are presented and the implications of the results are discussed in detail.

4.3.1.1 Early Age Compressive Strength Comparison – Flyash and Slag

The early age compressive strength results for Group 2 mixes are listed in Table 4.2 and Table 4.3, while the average compressive strengths are presented for comparison in Figure 4.1. Results show that the variation between the strengths of each batch is typically much higher at the earliest testing times, with the variation typically decreasing as the testing age increases. Additionally, the variation in strength for heat-blanket cured samples is significantly higher than normally cured samples at 6 hours, but this difference in variation becomes nonexistent by the 24 hour test. On average, the Slag mixes showed a higher strength development within the first 24 hours for both normal and heat-blanket curing when compared to the Flyash mixes. This difference is much more significant for heat-blanket curing, with a difference in strength of 10.5% for normal curing and 22.7% for heat-blanket curing. On average, the Flyash mixes had a higher increase in 6 hour compressive strength due to heat-blanket curing, while the Slag mixes had a higher increase in 24 hour compressive strength. Heat-blanket curing resulted in an average 6 hour compressive strength increase of 317% and 489% for Slag and Flyash mixes, respectively. For 24 hours, the increase in compressive strength is 34% and 18% for Slag and Flyash mixes, respectively. In comparison, G1-HPC-SL and G1-HPC-FA had a 24 hour strength of 4148 psi and 4419 psi, respectively.

Table 4.2 Early Age Compressive Strength of G2-HES-SL Mixes

Testing Time	HES-SL-A Initial Conc. Temp. = 79.1°F		HES-SL-B Initial Conc. Temp. = 80.4°F		HES-SL-C Initial Conc. Temp. = 74.8°F		Average Initial Conc. Temp. = 78.1°F (3.1%)	
	Normal Curing	Heat Blanket	Normal Curing	Heat Blanket	Normal Curing	Heat Blanket	Normal Curing	Heat Blanket
6hr	243	669	211	1370	231	812	228 (5.8%)	950 (31.8%)
7hr	538	1704	X	X	X	X	538**	1704**
8hr	951	3058	768	3846	1083	3695	934 (13.8%)	3533 (9.7%)
12hr	3495	5732	3097	5574	3774	5733	3455 (8.0%)	5680 (1.3%)
24hr	5972	7962	5812	7922	5932	7843	5905 (1.2%)	7909 (0.6%)

Table 4.3 Early Age Compressive Strength of G2-HES-FA Mixes

Testing Time	HES-FA-A Initial Conc. Temp. = 80.4°F		HES-FA-B Initial Conc. Temp. = 80.6°F		HES-FA-C Initial Conc. Temp. = 80.9°F		Average Initial Conc. Temp. = 80.6°F (0.3%)	
	Normal Curing	Heat Blanket	Normal Curing	Heat Blanket	Normal Curing	Heat Blanket	Normal Curing	Heat Blanket
6hr	159	565	243	1704	155	1019	186 (21.9%)	1096 (42.7%)
7hr	398	1597	X	X	X	X	398**	1597**
8hr	824	3121	1145	3683	748	3436	906 (19.0%)	3413 (6.7%)
12hr	3097	4897	3563	5374	2807	4666	3156 (9.9%)	4979 (5.9%)
24hr	5573	6688	5653	6529	4717	5673	5314 (8.0%)	6297 (7.1%)

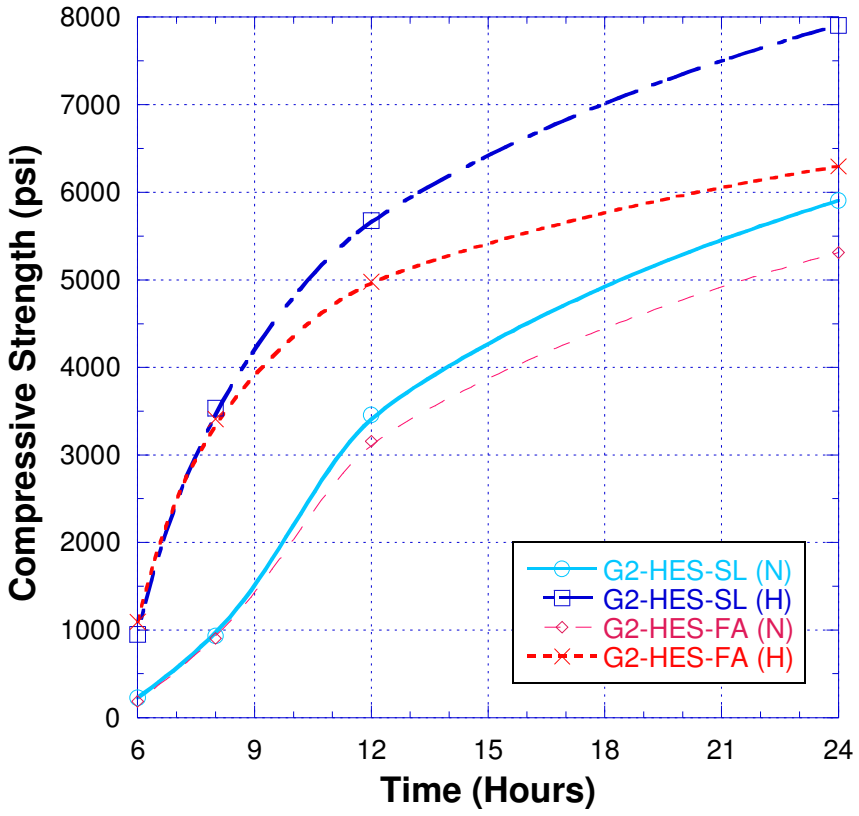

Figure 4.1 Early Age Compressive Strength of Group 2 mixes

The results for Group 3 mixes are presented below in Table 4.4 and Table 4.5, while the average compressive strengths are presented for comparison in Figure 4.2. Similarly to the Group 2 mixes, the Group 3 mixes show higher variations between batches at the earlier ages. Unlike the Group 2 mixes, the Group 3 mixes did not show a clear higher variation for the heat-blanket cured samples. As expected, the inclusion of SRA leads to a negative effect on the early age strength gain. For Slag mixes, the average decrease in the 6 hour compressive strength is 25.4% for normal curing, and 23.5% for heat-blanket curing. Flyash mixes show a much greater decrease in strength as a result of SRA, with an average decrease in the 6 hour compressive strength of 43.0% for normal curing, and 38.2% for heat-blanket curing. The effects are much less significant by the 24 hour compressive strength, with a decrease of 11.1% (normal curing) and 10.9% (heat-

blanket curing) for Slag mixes, and a decrease of 10.1% (normal curing) and 2.1% (heat-blanket curing) for Flyash mixes. Based on these results, SRA shows a greater effect on Flyash based mixes, as opposed to slag mixes, in the compressive strength at early ages. However, SRA's effects on the early age compressive strength of Flyash based mixes become similar to its effects on Slag based mixes by 24 hours.

Table 4.4 Early Age Compressive Strength of G3-SRA-SL Mixes

Testing Time	SRA-SL-A Initial Conc. Temp. = 78.5°F		SRA-SL-B Initial Conc. Temp. = 81.5°F		SRA-SL-C Initial Conc. Temp. = 83.9°F		Average Initial Conc. Temp. = 81.3°F (2.7%)	
	Normal Curing	Heat Blanket	Normal Curing	Heat Blanket	Normal Curing	Heat Blanket	Normal Curing	Heat Blanket
6hr	143	542	207	788	159	852	170 (16.0%)	727 (18.4%)
7hr	291	1975	X	X	X	X	291**	1975**
8hr	549	2799	860	3045	633	3265	681 (19.3%)	3036 (6.3%)
12hr	2731	5295	2962	4761	2890	5215	2861 (3.4%)	5090 (4.6%)
24hr	5195	6171	5215	7723	5334	7245	5248 (1.2%)	7046 (9.2%)

Table 4.5 Early Age Compressive Strength of G3-SRA-FA Mixes

Testing Time	SRA-FA-A Initial Conc. Temp. = 84.2°F		SRA-FA-B Initial Conc. Temp. = 86.4°F		SRA-FA-C Initial Conc. Temp. = 82.8°F		Average Initial Conc. Temp. = 84.5°F (1.8%)	
	Normal Curing	Heat Blanket	Normal Curing	Heat Blanket	Normal Curing	Heat Blanket	Normal Curing	Heat Blanket
6hr	108	828	139	573	72	629	106 (25.7%)	677 (16.2%)
7hr	263	2066	X	X	X	X	263**	2066**
8hr	553	3034	645	2691	322	3256	507 (26.8%)	2994 (7.8%)
12hr	2146	4523	2608	4097	1927	4359	2227(12.7%)	4326 (4.1%)
24hr	4857	5892	4877	6649	4598	5952	4777 (2.7%)	6164 (5.6%)

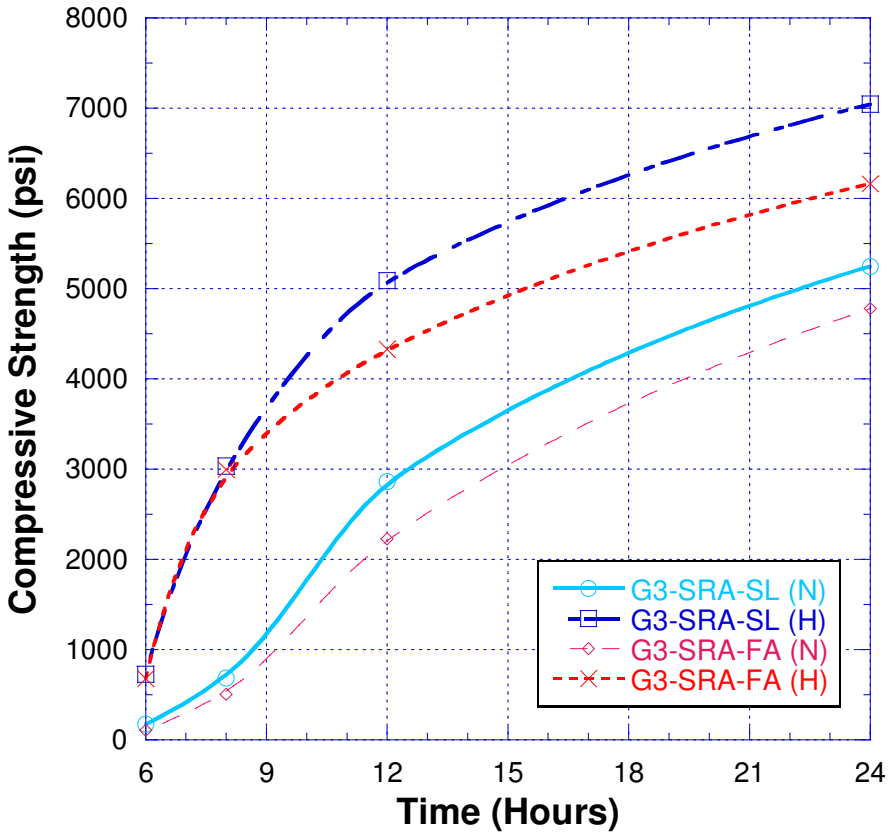

Figure 4.2 Early Age Compressive Strength of Group 3 mixes

4.3.1.2 Early Age Compressive Strength Comparison – HES and SRA

Figure 4.3 shows the comparison between the average strengths of the G2-HES-SL and G3-SRA-SL mixes. The inclusion of SRA lowers early age strength for both normal and heat curing. For normal curing the decrease in early age strength is 25.4%, 27.1%, 17.2%, and 11.1%, for 6 hour, 8 hour, 12 hour, and 24 hour testing, respectively. For heat curing the decrease in early age strength is 23.5%, 14.1%, 10.4%, and 10.9%, for 6 hour, 8 hour, 12 hour, and 24 hour testing, respectively. This shows that SRA's negative effect on strength becomes less significant as time goes on. It can also be seen that the decrease in strength is slightly greater for normal curing, as opposed to heat

curing. Furthermore, it should be noted that these results imply that mixes containing SRA can combat its decrease in early age strength by increasing the curing temperature.

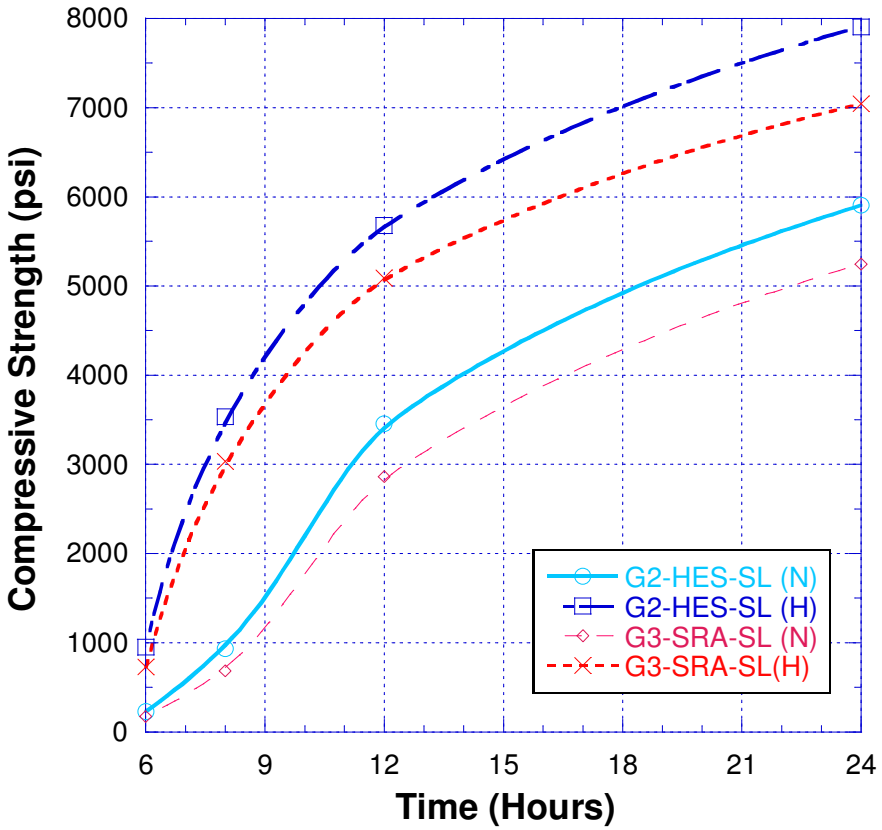

Figure 4.3 Average Early Age Compressive Strength, G2-HES-SL and G3-SRA-SL

Figure 4.4 shows the comparison between the average strengths of the G2-HES-FA and G3-SRA-FA mixes. Identically to the Slag mixes, SRA also produces lower early age strength for Flyash based mixes. For normal curing the decrease in early age strength is 43.0%, 44.0%, 29.4%, and 10.1%, for 6 hour, 8 hour, 12 hour, and 24 hour testing, respectively. For heat curing the decrease in early age strength is 38.2%, 12.3%, 13.1%, and 2.1%, for 6 hour, 8 hour, 12 hour, and 24 hour testing, respectively. The Flyash mixes show the same result as the Slag mixes, with the larger decrease in early age

strength being seen in the normally cured samples. Furthermore, the Flyash mixes show a much larger decrease in strength for normally cured samples compared to the Slag mixes.

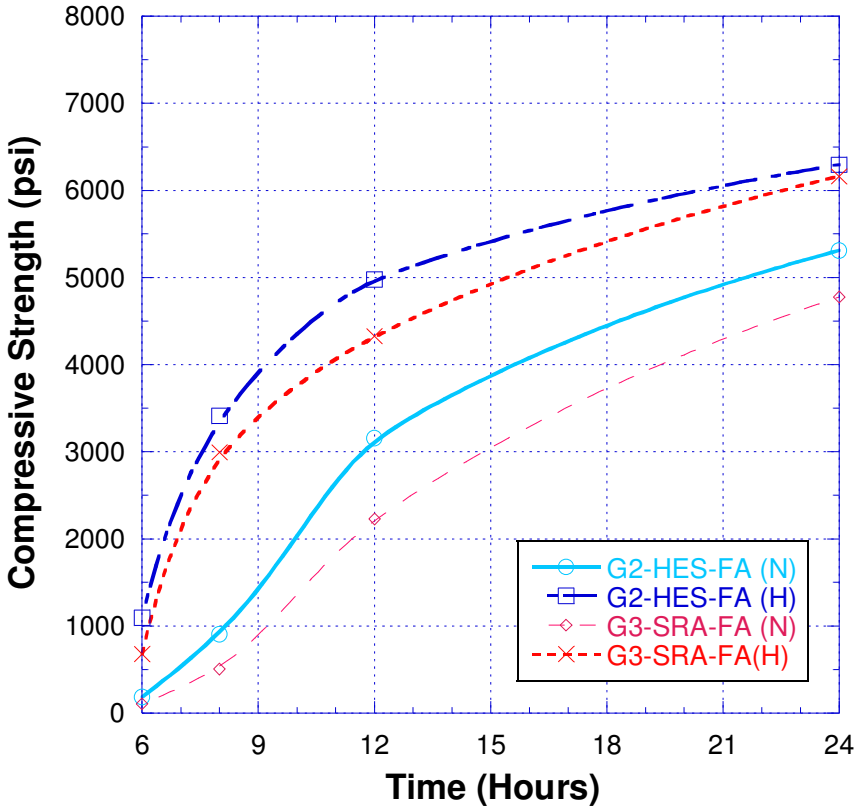

Figure 4.4 Average Early Age Compressive Strength, G2-HES-FA and G3-SRA-FA

4.3.2 Later Age Compressive Strength

For later age compressive strength, one batch per mix design was used, as the variation in compressive strength after 24 hours is minimal. Table 4.6 shows the later age compressive strength results of the Group 1 mixes. The results are what is typically expected of a HPC mix design. There is not a significant difference between the results of the Flyash mix and the Slag mix. However, it should be noted that the Flyash mix has a larger compressive strength at the 1 day testing age, while the Slag mix has a larger compressive strength at the 28 day testing age.

Table 4.6 Later Age Compressive Strength of Group 1 Mixes

Test Age	G1-HPC-SL	G1-HPC-FA
1 day	4148	4419
3 day	7006	6409
14 day	7444	7365
28 day	8758	8240

Table 4.7 shows the later age compressive strength results of the Group 2 and Group 3 mixes. Figure 4.5 presents the graph for Group 2 mixes, and Figure 4.6 presents the graph for Group 3 mixes. As shown in the table, the heat blanket cured results shows a lower 28 day strength than normal curing. This is a slightly more significant difference in the Group 3 mixes; approximately 4% and 7%, compared to approximately 2% in the Group 2 mixes. Also, SRA did not affect the 28 day strength much for the Slag based mixes, but did affect the Fly Ash mixes significantly. This implies SRA has a negative effect on 28 day strength of Fly Ash based mixes, but not on Slag based mixes. The normally cured G2-HES-SL showed a decrease in strength between 14 and 28 day, though this is assumed to be an error in the 14 day test, as the rest of results do not match with this outcome. This data point has been removed in constructing the graph to better present the strength curve.

Table 4.7 Later Age Compressive Strength of Group 2 and Group 3 Mixes

Age	G2-HES-SL		G2-HES-FA		G3-SRA-SL		G3-SRA-FA	
	Normal	1 day heat	Normal	1 day heat	Normal	1 day heat	Normal	1 day heat
1day	5905	7909	5314	6297	5248	7046	4777	6164
3day	8559	9554	7006	7325	7683	8272	6847	7365
14day	11306	10510	8917	8758	9644	9713	7763	7803
28day	10589	10430	10151	9952	11425	10629	9196	8838

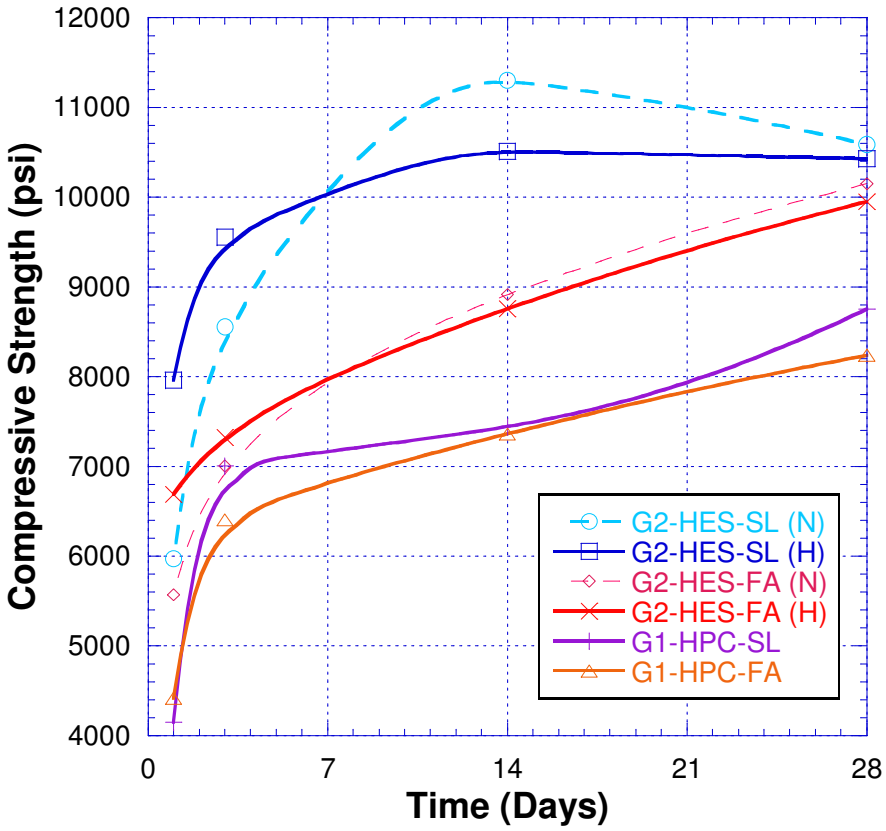

Figure 4.5 Later Age Compressive Strength for Group 2 Mixes

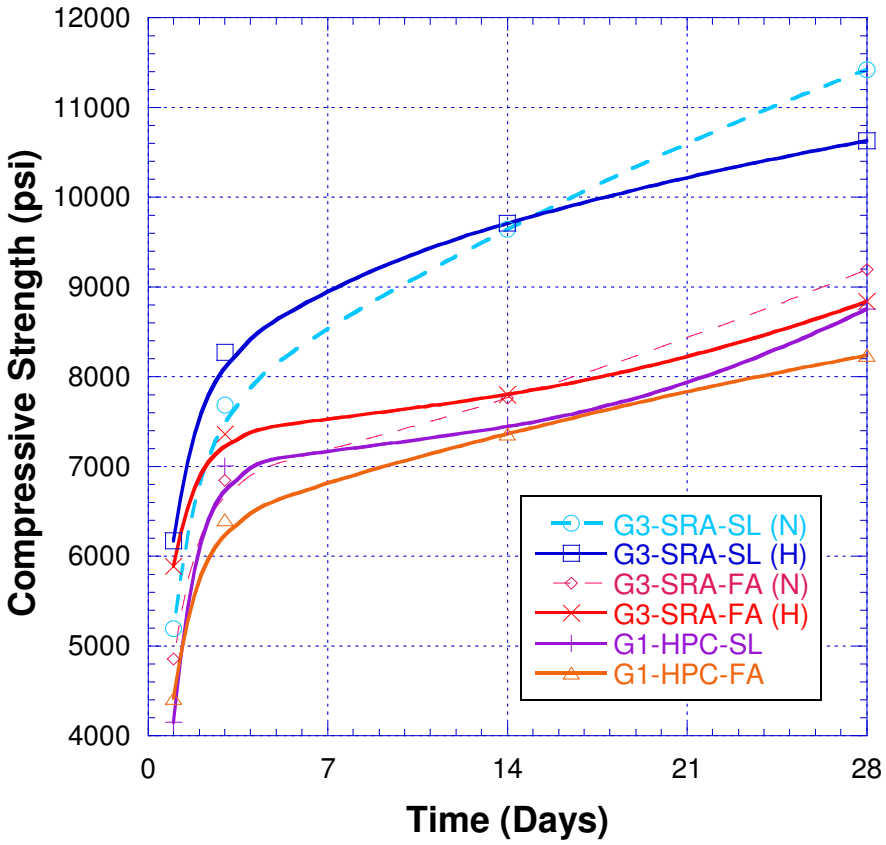

Figure 4.6 Later Age Compressive Strength for Group 3 Mixes

4.3.3 Splitting Tensile Strength

The splitting tensile strength results for the Group 1 mixes are presented in Table 4.8. The results of these mixes are generally proportional to the compressive strength results. For example, the Slag based mix has a higher compressive and splitting tensile strength than the Flyash mix at the 28 day testing age. The opposite is true for the 1 day test, where the Flyash mix has the larger compressive and splitting tensile strength.

Table 4.8 Splitting Tensile Strength of Group 1 Mixes

Test Age	G1-HPC-SL	G1-HPC-FA
1 day	313	344
3 day	375	363
14 day	433	430
28 day	502	471

The splitting tensile strength results for Group 2 and Group 3 mixes are presented in Table 4.9. Similarly to the Group 1 mixes, the results are typically proportional to the compressive strength results. Only one mix showed a higher tensile strength for heat curing compared to normal curing. The majority follows what is expected based on the compressive strength results, which shows a lower 28 day strength when heat curing is used. Overall, the tensile strength results do not appear to be consistent, with a decrease in strength seen at certain ages throughout the testing period. Furthermore, the variation between samples was within the limits presented by ASTM (less than 14%), but many mixes still had fairly high variation (8%-10%).

Table 4.9 Splitting Tensile Strength of Group 2 and Group 3 Mixes

Age	G2-HES-SL		G2-HES-FA		G3-SRA-SL		G3-SRA-FA	
	Normal	1 day heat	Normal	1 day heat	Normal	1 day heat	Normal	1 day heat
1day	405	508	380	527	342	481	365	435
3day	452	553	401	543	406	431	437	457
14day	667	619	574	470	X	X	495	503
28day	541	453	638	552	718	603	603	613

4.3.4 Modulus of Elasticity

For the modulus of elasticity, all mixes exhibited behavior that agrees with the compressive strength results. Typically when comparing normal and heat curing of the same mix, the results show a higher modulus of elasticity for heat curing during the 1 day

and 3 day test, similar results for the 14 day test, and lower results for the 28 day test. This trend is more or less identical to that of the compressive strength, which helps confirm both test results as accurate. Similarly to the splitting tensile strength results, most mixes showed a decrease in modulus of elasticity between the 14 day and 28 day tests.

Table 4.10 presents the results of the Group 1 mixes. Generally the results correlate well with the compressive and splitting tensile strength results for the corresponding mix, with a higher modulus of elasticity for higher strengths. Similarly to the compressive and splitting tensile strength results, the modulus of elasticity for G1-HPC-FA is larger at the 1 day test, while the modulus of elasticity for G1-HPC-SL is larger at the 28 day test. Additionally, the Group 1 mixes have a lower modulus of elasticity than their HES equivalent, which also displayed higher compressive strength results. The curves of the Group 1 mixes are included with those of the Group 2 and Group 3 mixes, in Figure 4.7 and Figure 4.8.

Table 4.10 Modulus of Elasticity of Group 1 Mixes

Test Age	G1-HPC-SL	G1-HPC-FA
1 day	3734	3925
3 day	4013	4394
14 day	4940	4766
28 day	5348	4909

Table 4.11 presents the results for the Group 2 and Group 3 mixes. Similarly to the Group 1 mixes, the test results correspond well with the compressive strength results. This is seen in the higher values at early ages for heat curing, and the higher values at later ages for normal curing. Identically to the compressive strength results, Slag mixes

have a higher 28 day modulus of elasticity than Flyash. Furthermore, there was a decrease in 28 day modulus of elasticity when SRA was added to the Slag mix, but not with the Flyash mix. The curves for modulus of elasticity are shown in Figure 4.7 and Figure 4.8.

Table 4.11 Modulus of Elasticity of Group 2 and Group 3 Mixes

Age	G2-HES-SL		G2-HES-FA		G3-SRA-SL		G3-SRA-FA	
	Normal	1 day heat	Normal	1 day heat	Normal	1 day heat	Normal	1 day heat
1day	4557	4724	4815	4842	4375	5070	3939	4452
3day	5378	5438	5515	5207	5364	5544	5045	4966
14day	6510	6176	5374	5577	X	X	5118	5186
28day	6296	5578	5300	5140	5624	5232	5136	5433

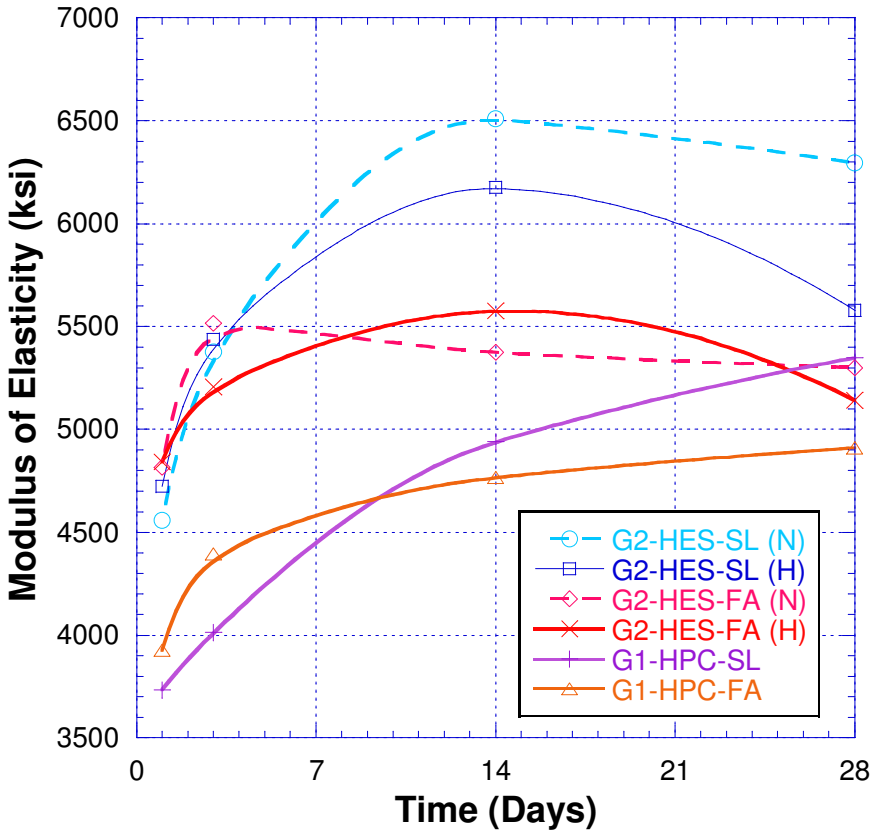

Figure 4.7 Modulus of Elasticity for Group 2 and Group 1 Mixes

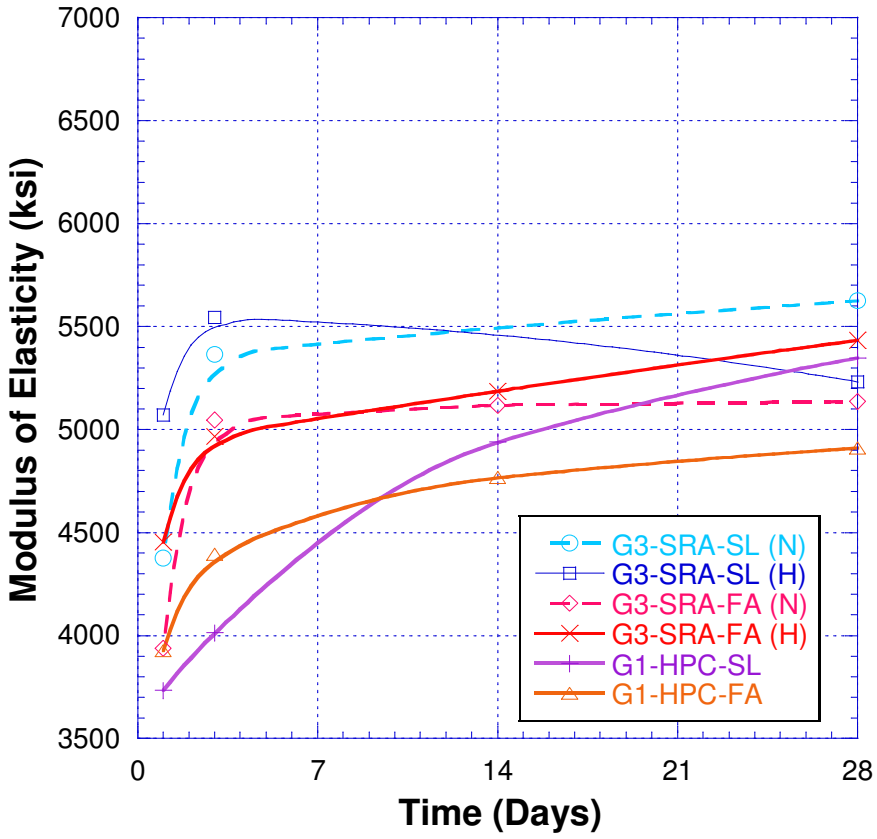

Figure 4.8 Modulus of Elasticity for Group 3 and Group 1 Mixes

4.3.5 Drying Free Shrinkage

The results of the drying free shrinkage for Group 1 mixes are presented in Table 4.12. Typical HPC mixes generally reach a free shrinkage strain between 350 μϵ and 600 μϵ, as seen in a previous study (Nassif, Najm, and Aktas, 2007), though it is found that larger quantities of pozzolan replacement will lead to an increase in free shrinkage strain. Since the mix designs in this study did not use a very high pozzolan replacement for Slag or Flyash, both HPC mixes resulted in a free shrinkage value of approximately 350 μϵ by the 91 day testing schedule. Between 56 and 91 days, the concrete is still experiencing an increase in free shrinkage strain, though not by a significant quantity.

Table 4.12 Drying Free Shrinkage for Group 1 Mixes

Age	G1-HPC-SL	G1-HPC-FA
14 day	0	0
15 day	-35	-40
16 day	-70	-75
17 day	-	-
18 day	-	-
19 day	-125	-145
20 day	-140	-175
21 day	-160	-205
28 day	-210	-240
42 day	-265	-290
56 day	-325	-330
91 day	-350	-355

The results of the drying free shrinkage for Group 2 and Group 3 mixes are presented in Table 4.12, while the curves are presented in Figure 4.9 and Figure 4.10. As seen by the table, G2-HES-SL continued to experience increased shrinkage between the 56 day and 91 day tests. This is equally significant for the samples that have undergone 1 day heat-blanket curing and normal curing, which experiences a 14.7 % increase in strain and a 16.1% increase in strain during this time, respectively. By adding SRA in the mix proportions, the 91 day free shrinkage strain decreases by 49.2% for normal curing and 42.3% for 1 day heat-blanket curing. Furthermore, the increase in strain between the 56 day and 91 day test is 6.5% for normal curing and 2.3% for 1 day heat-blanket curing. So the inclusion of SRA leads to a significant decrease in 91 day shrinkage, and had a significant decrease in the rate of shrinkage between 56 and 91 days. For the Flyash based mixes, SRA had a much less significant effect on reducing shrinkage. SRA reduced the 91 day drying shrinkage by 25.7% and 17.5% for normal and heat-blanket curing, respectively.

Table 4.13 Drying Free Shrinkage for Group 2 and Group 3 Mixes

Age	G2-HES-SL		G2-HES-FA		G3-SRA-SL		G3-SRA-FA	
	Normal	1 day heat	Normal	1 day heat	Normal	1 day heat	Normal	1 day heat
14 day	0	0	0	0	0	0	0	0
15 day	-35	-60	-65	-85	-20	-20	-50	-55
16 day	-70	-115	-100	-115	-50	-40	-	-
17 day	-	-	-120	-130	-65	-70	-110	-130
18 day	-	-	-140	-155	-	-	-	-
19 day	-145	-190	-	-	-	-	-	-
20 day	-155	-205	-	-	-95	-115	-140	-150
21 day	-175	-215	-170	-190	-120	-140	-180	-155
28 day	-205	-270	-185	-220	-125	-175	-205	-215
35 day	-	-	-225	-255	-140	-200	-225	-265
42 day	-225	-295	-250	-280	-155	-215	-265	-295
49 day	-	-	-285	-305	-	-	-270	-295
56 day	-280	-340	-320	-345	-155	-220	-270	-305
91 day	-325	-390	-370	-400	-165	-225	-275	-330

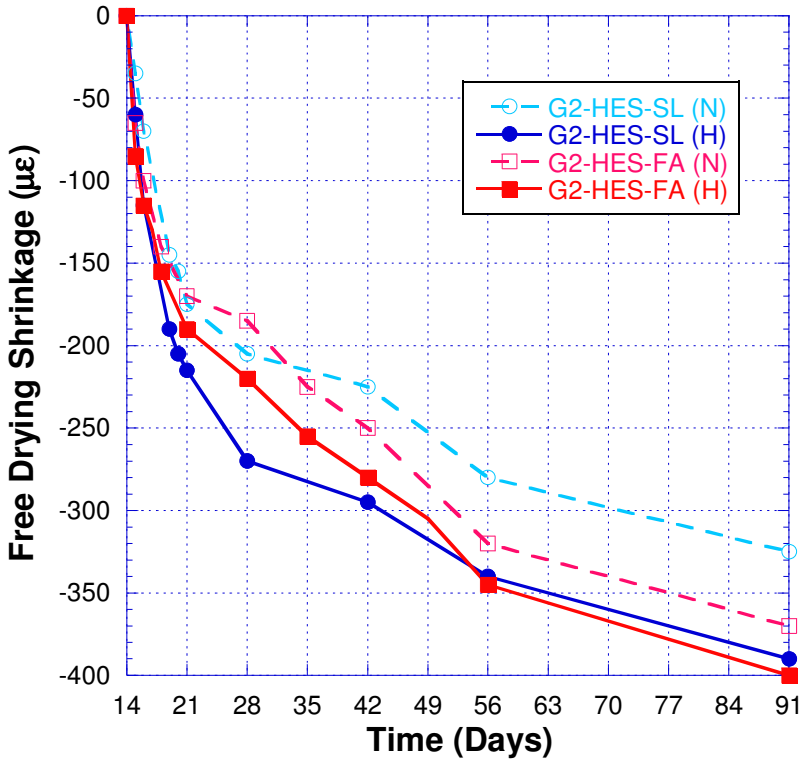

Figure 4.9 Free Drying Shrinkage for Group 2 Mixes

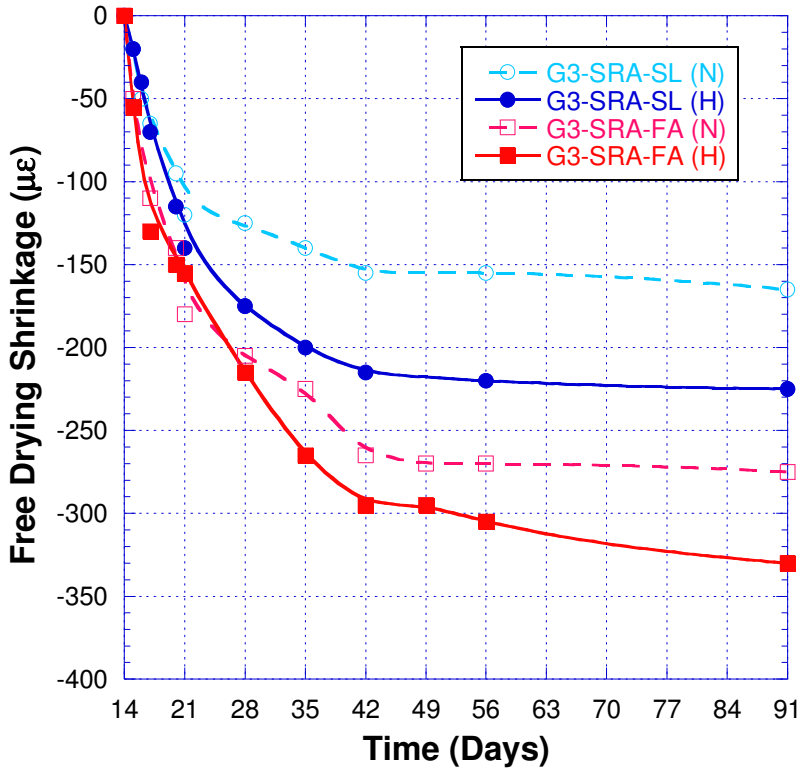

Figure 4.10 Free Drying Shrinkage for Group 3 Mixes

4.4 RESTRAINED SHRINKAGE

The results of the modified AASHTO PP34 restrained shrinkage test are presented below. Comparisons are made between the results of the steel strains and the concrete strains. The results of the VWSG readings should correlate with the FSG readings; with the correct sensor of each gage signaling a crack or not. Although previous studies have monitored the restrained shrinkage test for longer than 56 days, it is believed that any mix that does not crack within 56 days is considered to be adequate at resisting restrained shrinkage cracking. By limiting the test to 56 days it allows one laboratory to sample restrained shrinkage rings much more often. Furthermore, based on the free shrinkage test results, the concrete shows a minimal increase in shrinkage strain between 56 and 91 days. In addition to monitoring any cracks that penetrate through the entirety of the thickness of the ring, number and length/width of cracks can be monitored for comparison. The early age behavior and the drying shrinkage behavior are examined.

4.4.1 Early Age Shrinkage Behavior

During the 14 day curing period, the rings are kept under wet burlap in the environmental chamber. It is important to monitor the early age behavior of the shrinkage strains to determine if there exists any autogenous shrinkage. Because the wet burlap is placed directly on the VWSGs embedded in the concrete, it is better to monitor the FSGs on the steel as the burlap may affect the results of the strain readings. Figure 4.11 presents the early age behavior of the strain in steel for normal and heat-blanket curing for mix G2-HES-FA. As seen in the figure, heat-blanket curing leads to more eradicate readings and shows more expansion in the steel due to the high temperature under the blanket. The normally cured ring shows some early expansion due to the heat of

hydration but returns to a reading of zero strain for the remainder of the curing period. For the heat-blanket cured sample, two of the gauges show some shrinkage by day 3, but this did not actually lead to a higher strain in the steel by day 21. This confirms previous studies which have shown proper curing leading to the elimination of autogenous shrinkage.

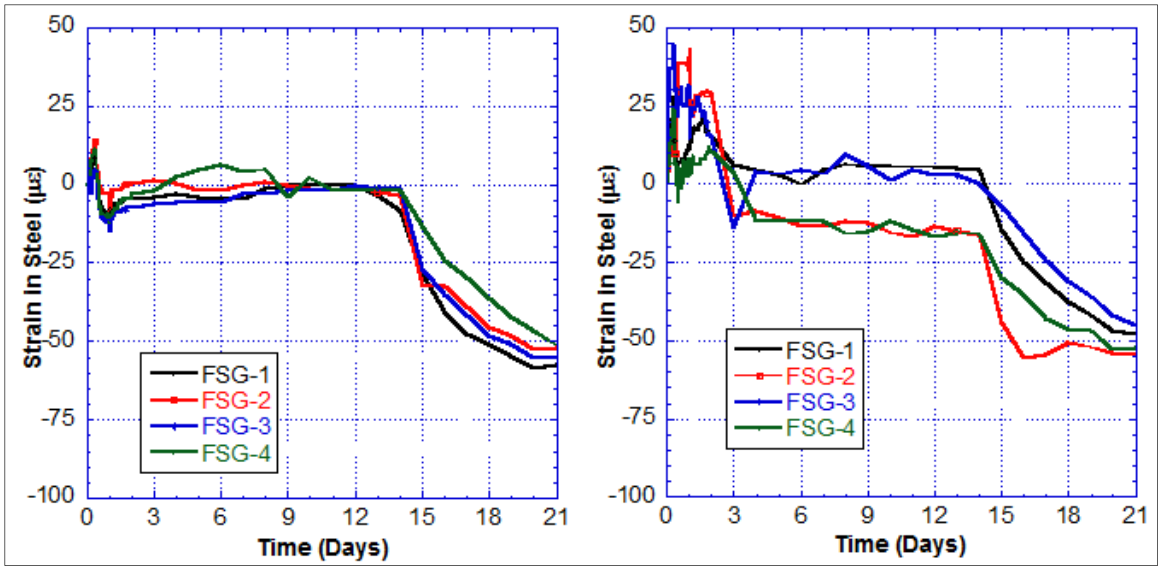

Figure 4.11 Early Age Shrinkage Behavior for normal (left) and heat-blanket curing (right) for G2-HES-FA

4.4.2 Post-Curing VWSG and FSG Readings

Once the rings are done curing for 14 days, the burlap is removed and the ring begins going through drying shrinkage. This initiates the start of crack monitoring, along with the monitoring of the VWSG and FSG readings, which can help indicate when and where a crack occurs. Generally, restrained shrinkage cracks occur at the top edge of the concrete ring and over time will penetrate through to the steel ring. A jump in one of the steel ring strains indicates a crack occurring near that side of the ring, while a VWSG

reading surpassing the cracking strain will indicate a crack near that side of the concrete ring.

Figure 4.12 and Figure 4.13 present the results of the VWSG readings for G1-HPC-SL and G1-HPC-FA, respectively. Despite a relatively low cracking strain, neither ring shows any VWSG readings that reach this strain, which indicates no significant restrained shrinkage crack penetrates through the concrete ring. As will be shown in the Group 2, the Group 1 mixes show lower strain readings and less cracking in the crack maps. The cracking behavior will be discussed in more detail in the section to follow. If the test were to continue and the concrete continued to shrink, the location of VWSG-4 for G1-HPC-SL would likely be the location of cracking. For G1-HPC-FA, the location of VWSG-1 and VWSG-2 would likely be the location of cracking.

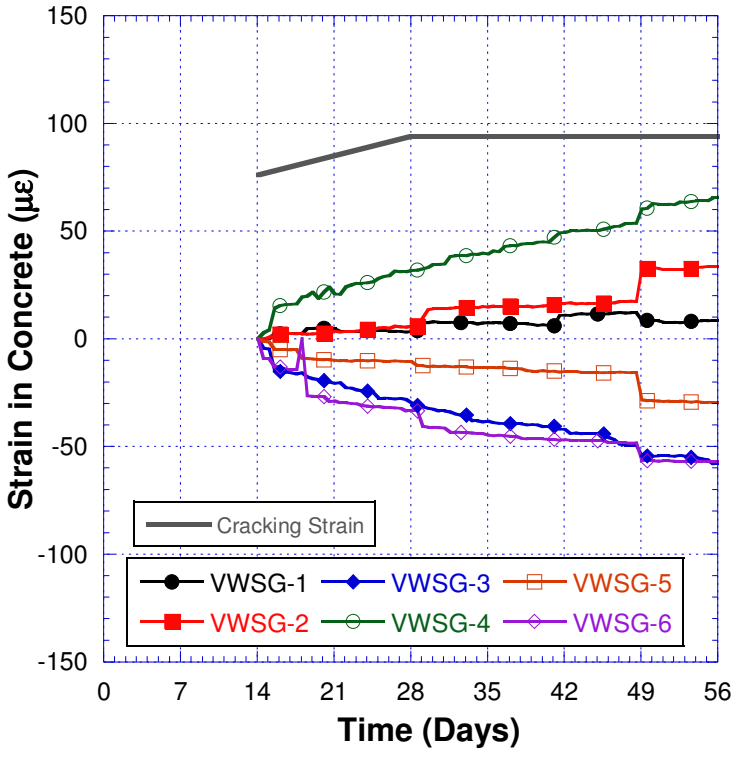

Figure 4.12 VWSG Readings for G1-HPC-SL

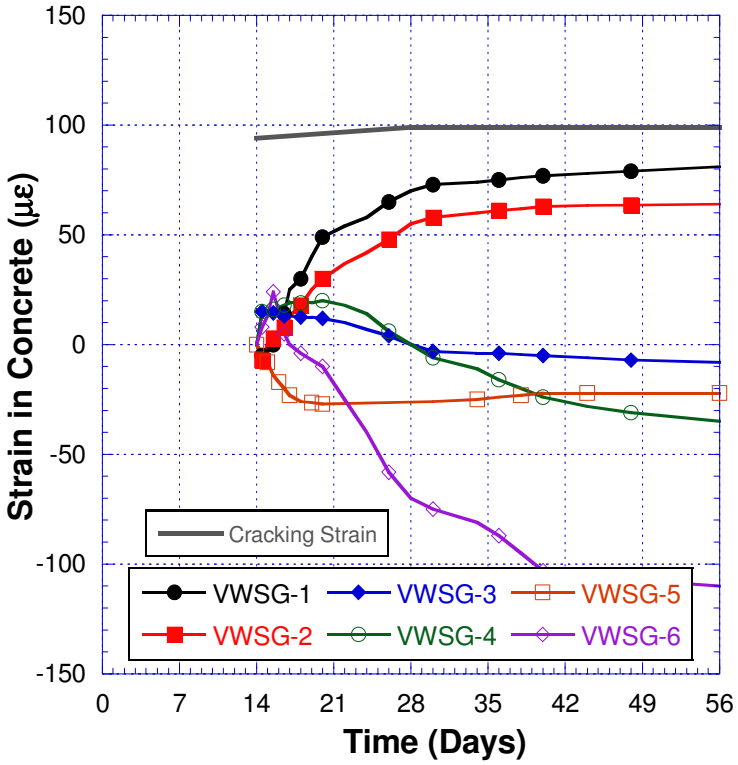

Figure 4.13 VWSG Readings for G1-HPC-FA

Figure 4.14 presents the VWSG strain readings with the VWSG and FSG setup for the normally cured G2-HES-SL, while Figure 4.15 presents the FSG strain readings. As seen in the VWSG readings, VWSG-6 read a strain above the cracking strain at approximately 22 days. Similarly, the strain reading of FSG-2 shows a change in its trend at approximately 23 days, with a temporary increase in strain, followed by eradicate strain readings that fluctuate as it steadily decreases more slowly than the other FSG. Compared to FSG-3, FSG-2 follows the same trend prior to 22 days, and then seems to compress at a much slower rate following the initiation of the crack, likely implying that the crack has helped release some of the stress through the crack. The diagram in Figure 4.14 shows that VWSG-6 is at the same location on the ring as FSG-2. Additionally, a crack was seen at this location on the 24th day, which then had fully propagated to the

steel by the 28th day. The crack map for this and all other rings will be shown in the following section. For the normally cured ring of G2-HES-SL, the FSG and VWSG correlated very well, with a nearly identical age-to-cracking.

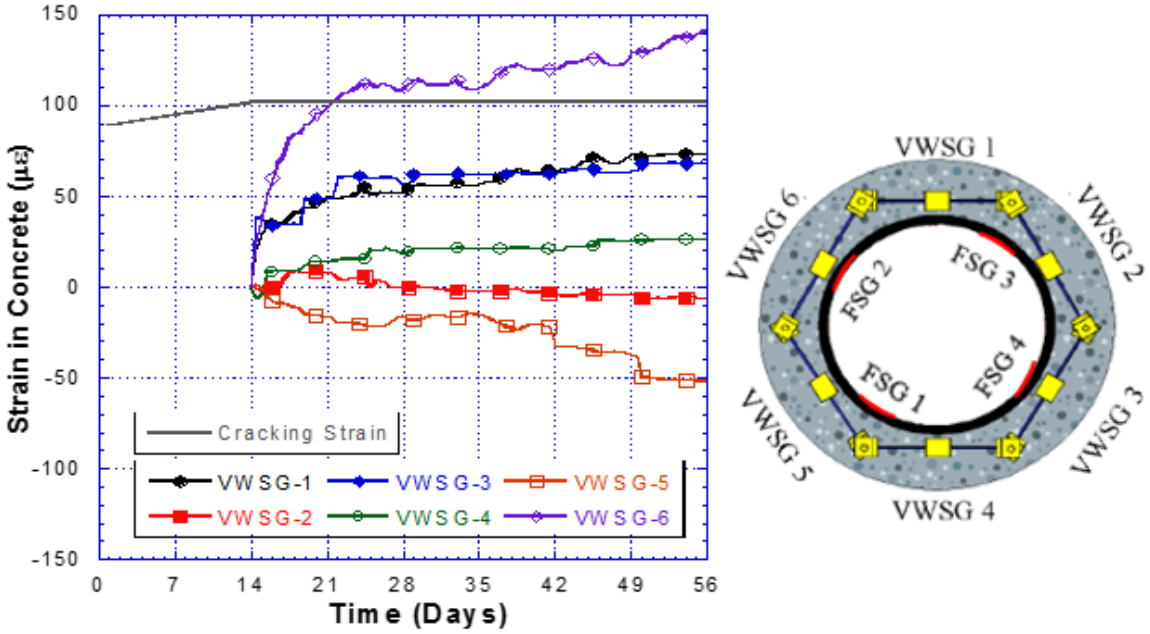

Figure 4.14 VWSG - Strain in Concrete for G2-HES-SL (N)

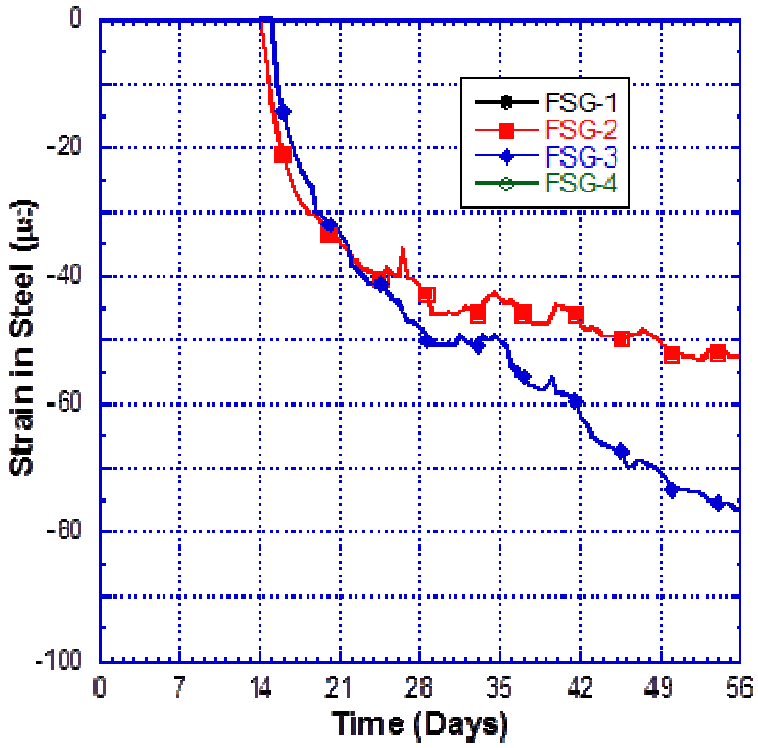

Figure 4.15 FSG - Strain in Steel for G2-HES-SL (N)

Figure 4.16 presents the VWSG strain readings with the VWSG and FSG setup for the 1 day heat blanket cured G2-HES-SL, while Figure 4.17 presents the FSG strain readings. Unlike the normally cured ring, the 1 day heat blanket cured ring does not show a VWSG reading that reaches the cracking strain. This would indicate that no crack occurred to reach through the thickness of the ring. VWSG-4 appears to have the highest tensile strain reading, which indicates that it is most likely to be the location of a crack propagating throughout the thickness of the concrete. On the other hand, FSG-2 shows an increase in strain between 24 days and 28 days, before following the trends of the other FSGs. This may indicate that some stress was released through a crack, but this did not release enough stress to prevent the steel from continuing to be compressed at an equal rate. This can be explained by the crack map, which shows multiple cracks appearing at

the steel ring, but do not penetrate throughout the entire concrete ring. This is not how the ring typically cracks, which may be the cause of the FSG not matching up with its corresponding VWSG. These results will be discussed further along with the crack map in the section to follow.

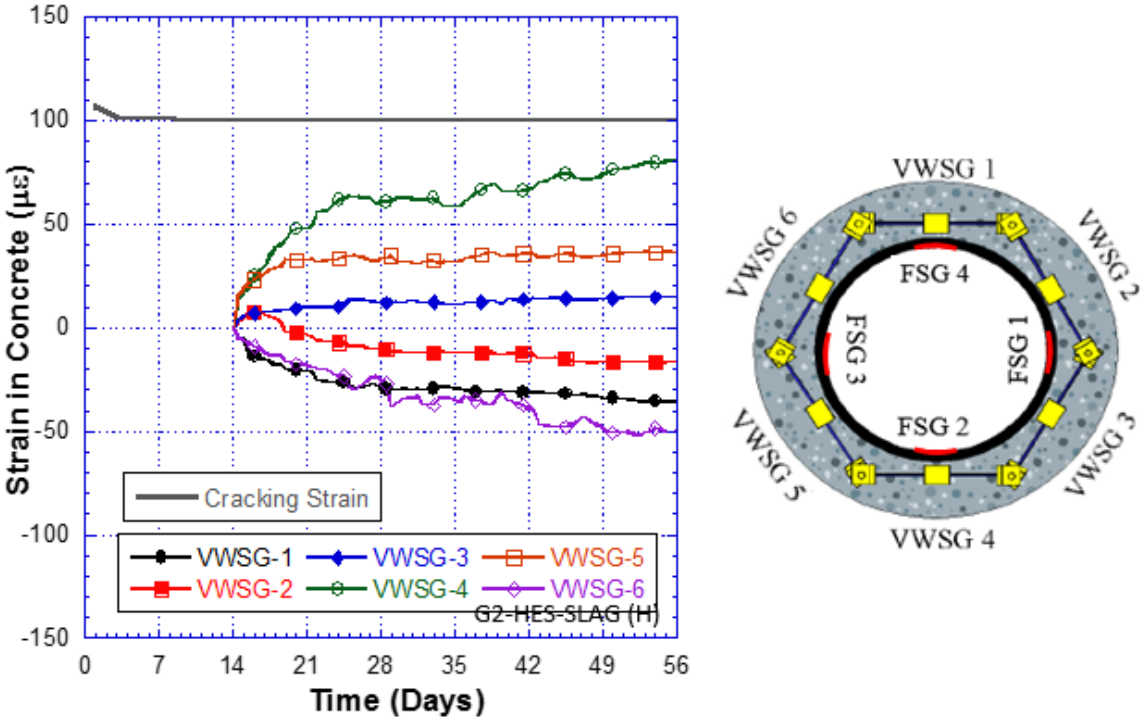

Figure 4.16 VWSG - Strain in Concrete for G2-HES-SL (H)

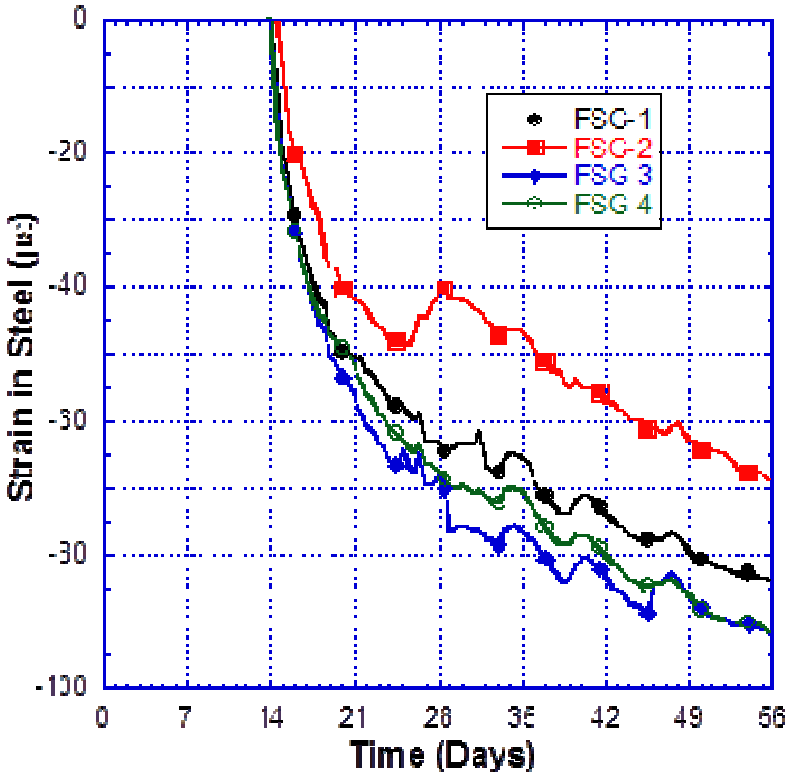

Figure 4.17 FSG - Strain in Steel for G2-HES-SL (H)

Figure 4.18 presents the VWSG strain readings with the VWSG and FSG setup for the normally cured G2-HES-FA, while Figure 4.19 presents the FSG strain readings. From the VWSG readings, VWSG-5 showed a strain reading greater than the cracking strain at approximately day 35. The corresponding FSG, FSG-4, showed a sharp increase on day 32, followed by erratic strain readings until 56 days. FSG-1 also showed a slight decrease in strain at day 35. This agrees with the crack map results, where a crack penetrated throughout its thickness. However, because the crack did not penetrated throughout the depth of the ring, two of the FSGs showed a release in strain followed by an increase in strain. Furthermore, the VWSG correctly identified the location of the crack.

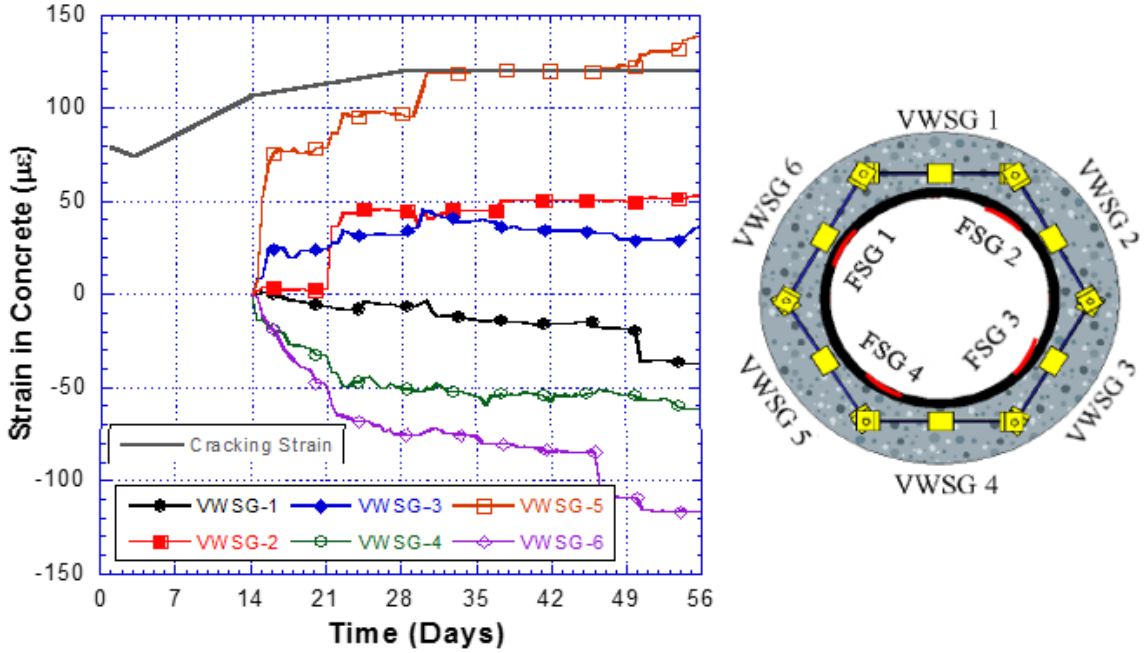

Figure 4.18 VWSG - Strain in Concrete for G2-HES-FA (N)

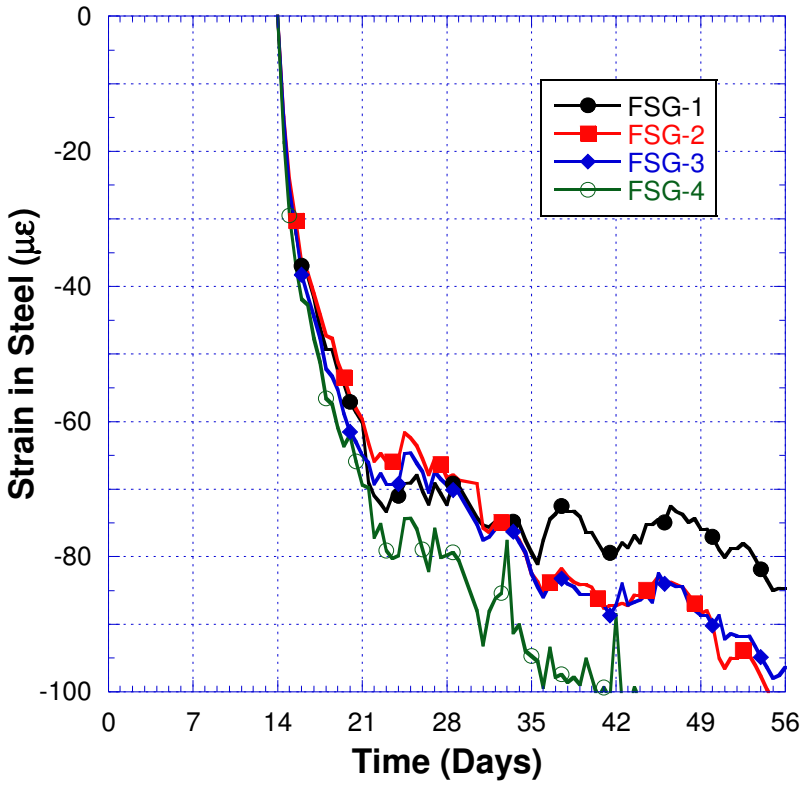

Figure 4.19 FSG - Strain in Steel for G2-HES-FA (N)

Figure 4.20 presents the VWSG strain readings with the VWSG and FSG setup for the 1 day heat blanket cured G2-HES-FA, while Figure 4.21 presents the FSG strain readings. Both sets of strain gages showed lower strain readings than the normally cured ring. The gages indicate that no restrained shrinkage cracks were formed, which agrees with the results of the crack map. Despite slightly higher free drying shrinkage results (7.8%), the heat-blanket cured ring did not show a restrained shrinkage crack. It also showed a 20% decrease in 56 day strain, according to the FSGs.

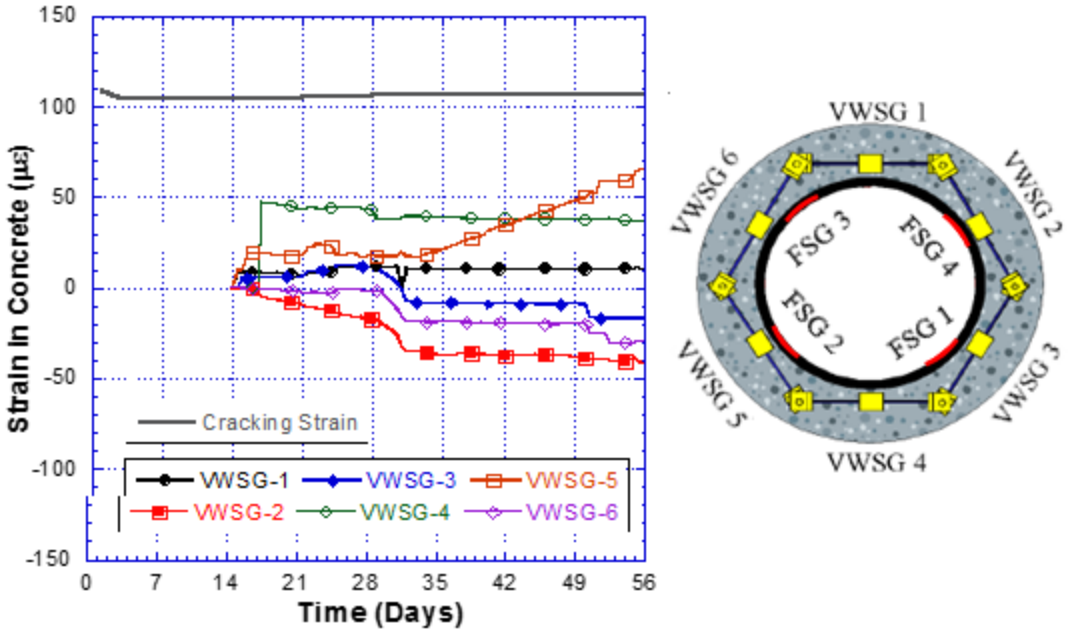

Figure 4.20 VWSG - Strain in Concrete for G2-HES-FA (H)

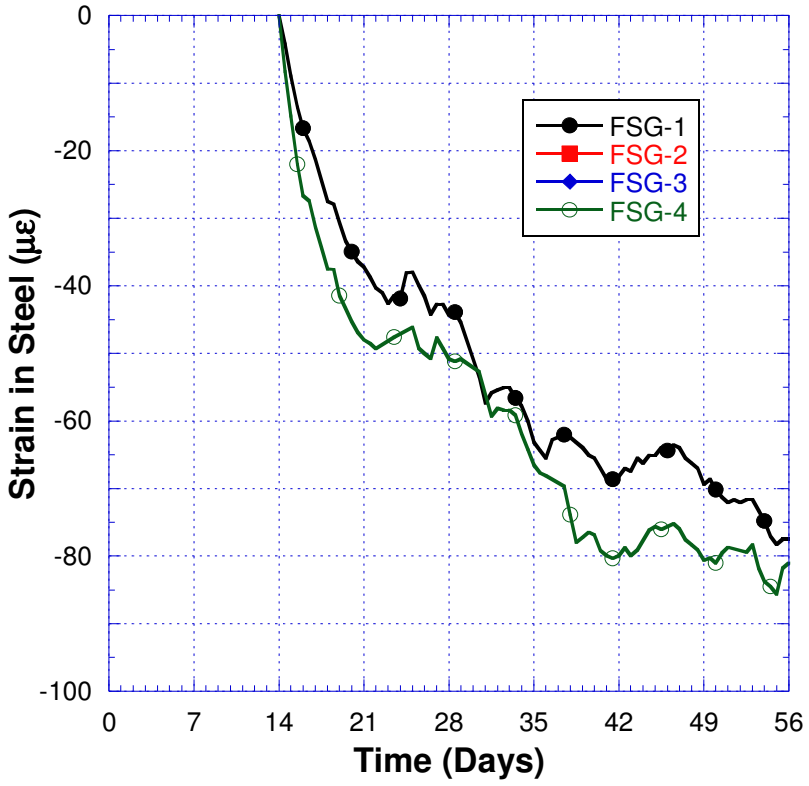

Figure 4.21 FSG - Strain in Steel for G2-HES-FA (H)

Figure 4.22 presents the VWSG strain readings with the VWSG and FSG setup for the normally cured G3-SRA-SL, while Figure 4.23 presents the FSG strain readings. Based on the results, no strain reading is observed to surpass the cracking strain, unlike the same mix which does not include SRA. However, the strain values are not significantly smaller than the HES-Slag mix, but does show no significant changes in strain values by day 21. VWSG-3 shows the highest tensile strain value, indicating this location as the most likely to crack. However, due to neither reaching the cracking strain, the ring should not show cracking in the crack map. The FSGs also show similar trends in the changes in strain, which also indicates no crack occurred within the 56 day testing period.

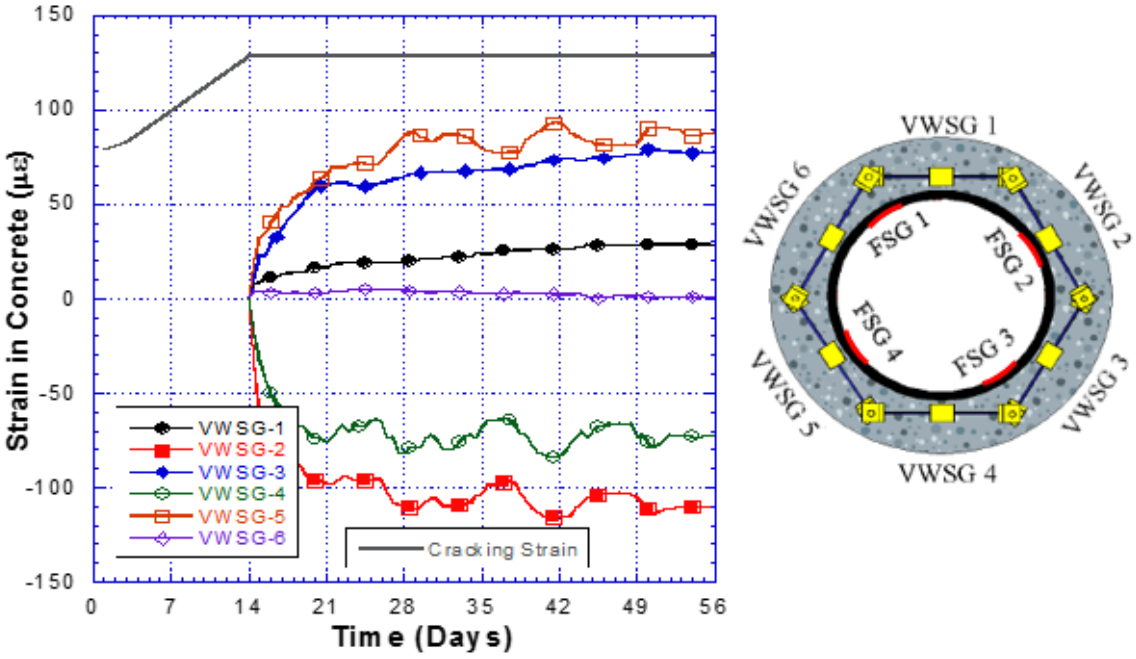

Figure 4.22 VWSG - Strain in Concrete for G3-SRA-SL (N)

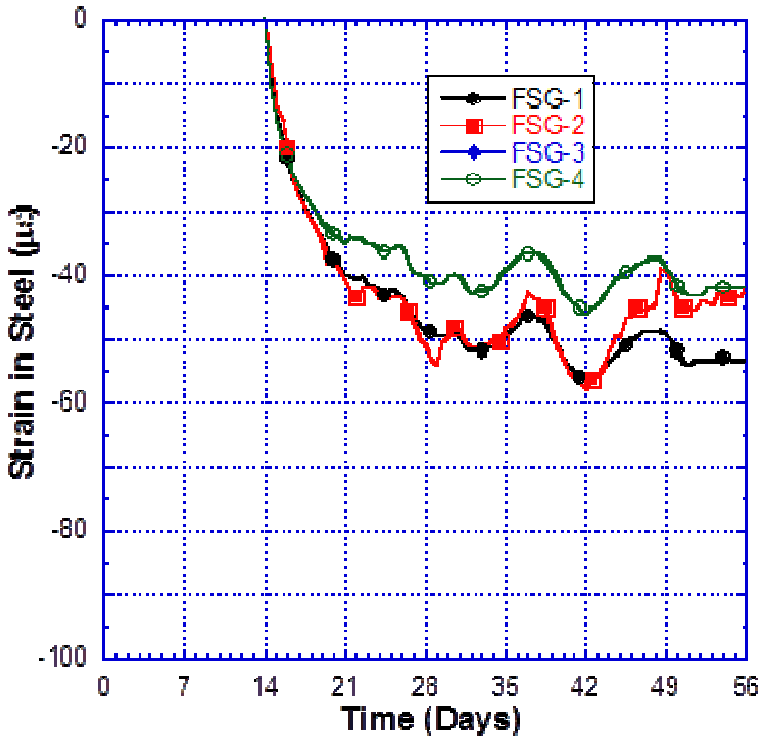

Figure 4.23 FSG - Strain in Steel for G3-SRA-SL (N)

Figure 4.24 presents the VWSG strain readings with the VWSG and FSG setup for the 1 day heat blanket cured G3-SRA-SL, while Figure 4.25 presents the FSG strain readings. Similarly to the normally cured ring, the heat blanket curing did not seem to lead to the ring cracking based on the VWSG readings. In fact, only one of the strain readings showed a compressive or tensile strain of more than 50 με. Unusually, the FSGs showed higher strain readings for this ring than the others, but all FSGs showed no sign of stress being released through cracking. No cracks penetrated through the entirety of the ring, though the side of the ring with the highest concentration of micro-cracks matches up with VWSG-1 and FSG-1. In the VWSG graph, VWSG-1 is the only gauge to indicate a moderate jump in tensile strain. FSG-1 shows no difference in the strain trend between the other gauges, indicating no crack reaching the steel. The relationship of these two indicates that over time if the strain reading in VWSG-1 were to continue to increase, eventually a crack would penetrate to the steel, which would then be signaled by FSG-1. These results will be discussed further, along with the crack maps, in the section to follow.

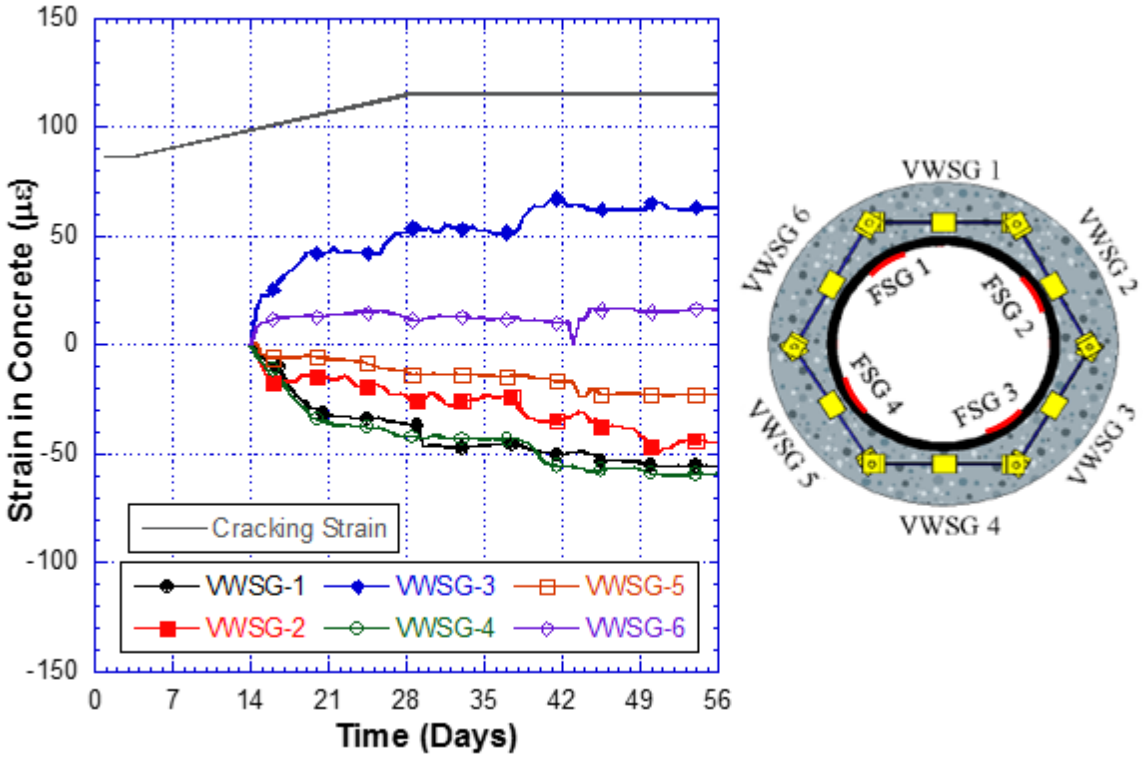

Figure 4.24 VWSG - Strain in Concrete for G3-SRA-SL (H)

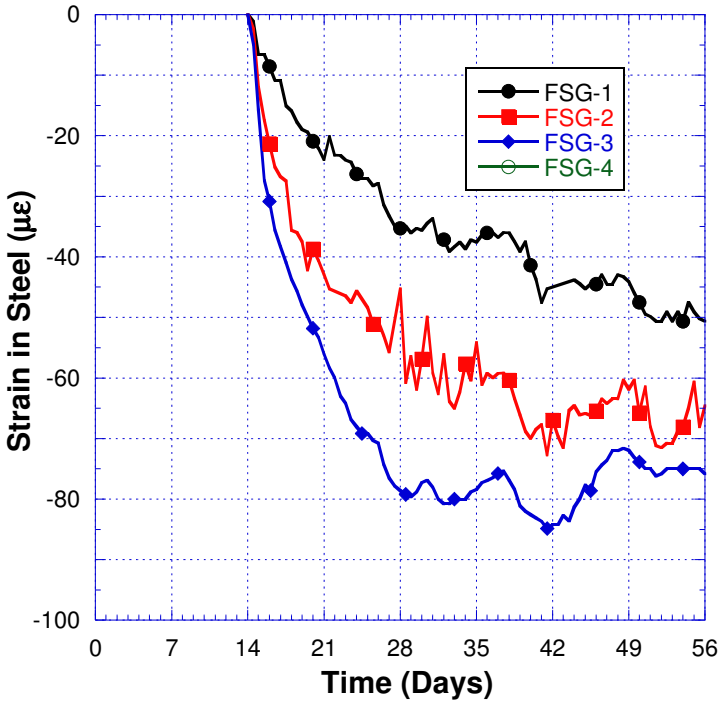

Figure 4.25 FSG - Strain in Steel for G3-SRA-SL (H)

Figure 4.26 presents the VWSG strain readings with the VWSG and FSG setup for the normally cured G3-SRA-FA, while Figure 4.27 presents the FSG strain readings. Similarly to the SRA-SLAG mix, the normally cured G3-SRA-FA shows lower strain readings than its HES Flyash counterpart. It also shows an insignificant change in strain readings by day 21. VWSG-3 and VWSG-6 show the highest tensile strain value by the end of the 56 day testing period, but neither reaches the cracking strain. This does not agree with the crack map, which did show a crack near VWSG-6 and FSG-4. However, FSG-4 does not show any sign of cracking, which indicates that the crack did not propagate all the way to the steel. The VWSG readings did not indicate a crack however, possibly because the crack occurred at the connection of VWSG-6 and VWSG-1. It is safe to assume that the crack did not affect either strain gauge.

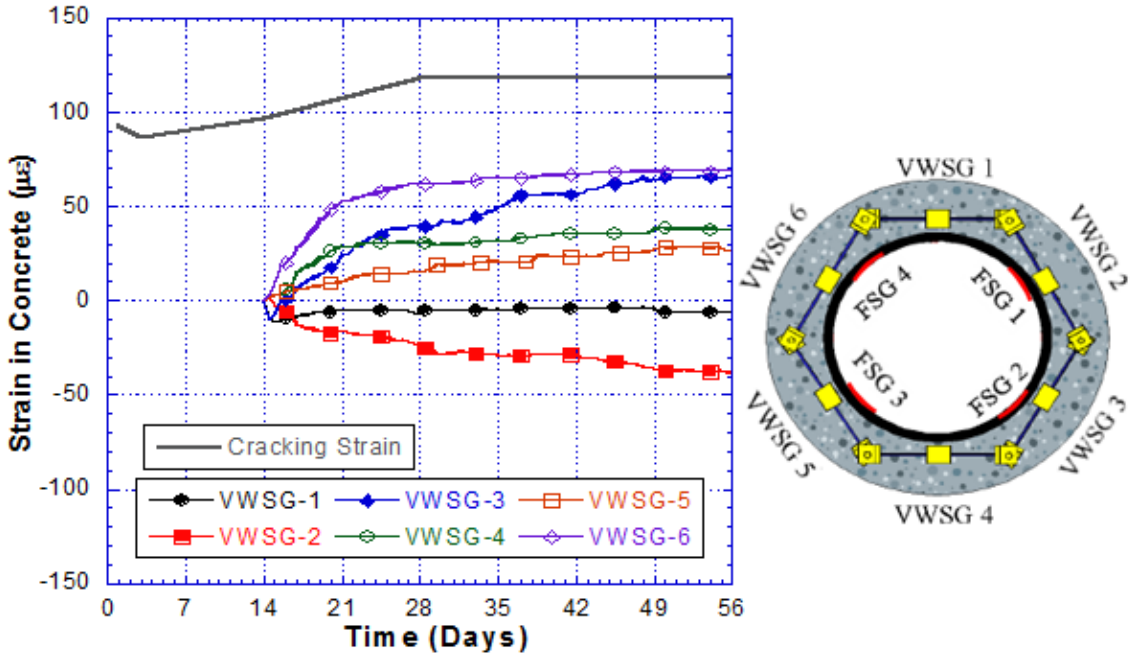

Figure 4.26 VWSG - Strain in Concrete for G3-SRA-FA (N)

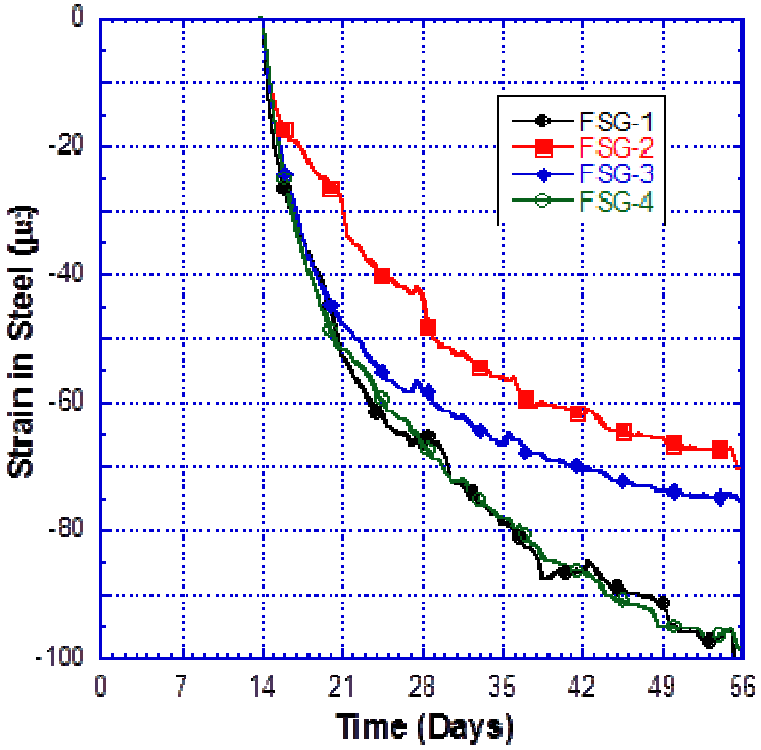

Figure 4.27 FSG - Strain in Steel for G3-SRA-FA (N)

Figure 4.28 presents the VWSG strain readings with the VWSG and FSG setup for the normally cured G3-SRA-FA, while Figure 4.29 presents the FSG strain readings. The VWSG and FSG data showed no sign of cracking. At day 42, VWSG-1 experiences some increase in tensile strain while the corresponding FSG, FSG-1, also shows a slight difference in its trend. This is not significant enough to indicate any restrained shrinkage cracks, but does show how well the two gages can correlate. It also indicates that if the ring were to crack in the future, this would be the section of the ring to do so. Unlike the normally cured ring, the heat-blanked cured ring did not experience a crack propagating to the steel. Though this was believed to be because of the bolt, as this was where the

crack was located. These results will be discussed further, along with the crack maps, in the section to follow.

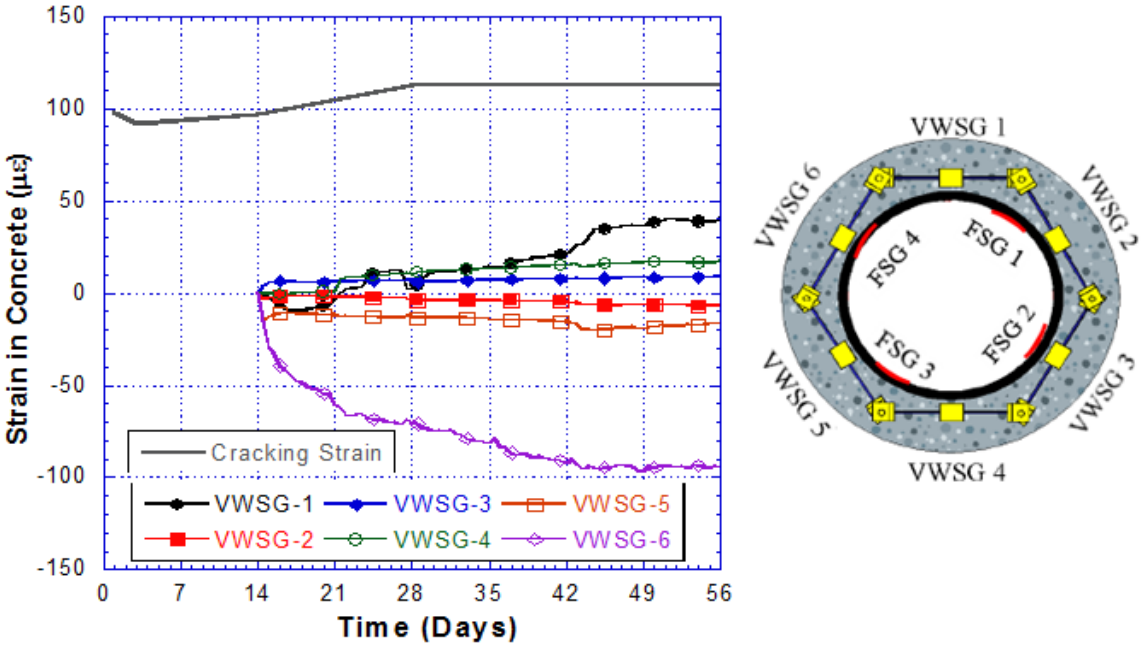

Figure 4.28 VWSG – Strain in Concrete for G3-SRA-FA (H)

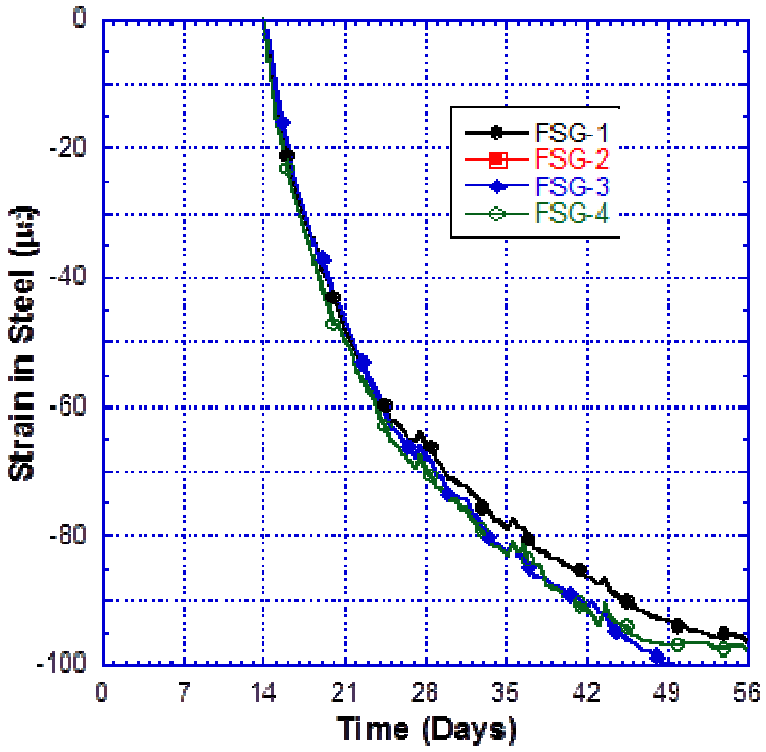

Figure 4.29 FSG - Strain in Steel for G3-SRA-FA (H)

4.4.3 Cracking Behavior Comparison – Normal and Heat-Blanket Curing

Cracking is monitored periodically with a digital microscope, with all cracks being recorded for day they were found, the length, and the width. The entirety of the ring was scanned for cracks on days 21, 28, 42, and 56. However, the ring was also checked for cracking in the area of any VWSG or FSG which signaled cracking. Crack maps are provided in this section to compare the cracking development of rings. This includes comparisons between total number of cracks, cracking rate, and number of significant cracks (i.e. cracks penetrating through the concrete to the steel).

Table 4.14 below presents the crack growth behavior of the Group 1 mixes, by comparing the number of cracks at various ages. There appears to be no significant difference in the crack patterns of the Slag and Flyash based HPC mixes.

Table 4.14 Crack Growth in Group 1 Mixes

Age	Number of Cracks	
	G1-HPC-SL	G1-HPC-FA
21	3	2
28	6	8
42	8	10
56	4	4
Total	21	24

The crack maps of the Group 1 mixes are presented in Figure 4.30 and Figure 4.31 for G1-HPC-SL and G1-HPC-FA, respectively. Both mixes share similar cracking behavior, with the most cracking occurring between day 28 and day 42. By 56 days the ring is still experiencing more cracking, but does not appear to be significant. Neither ring experiences any crack that penetrated throughout the top of the ring. The most severe crack for G1-HPC-SL was mapped at day 42 with a width of .03 mm and a length of 32 mm. The most severe crack for G1-HPC-FA was also mapped at day 42 with a width of .03 mm and a length of 16 mm. Since neither ring experienced a crack propagating to the steel, neither ring should have any FSG or VWSG signaling a restrained shrinkage crack. As will be seen below, the HPC mix designs lead to lower cracking when compared to HES concrete, probably due to the effects of the accelerated curing of HES concrete.

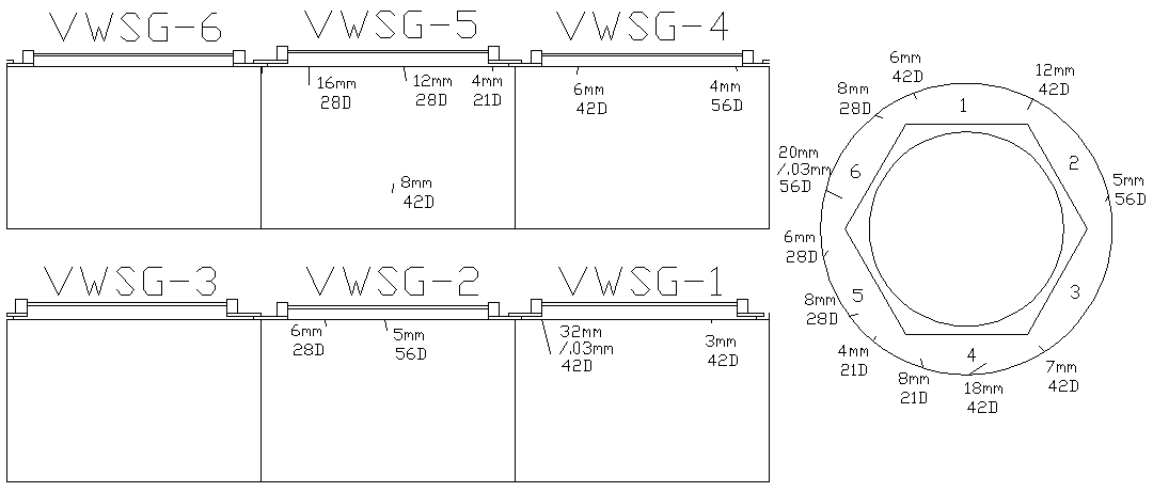

Figure 4.30 Crack Map of G1-HPC-SL

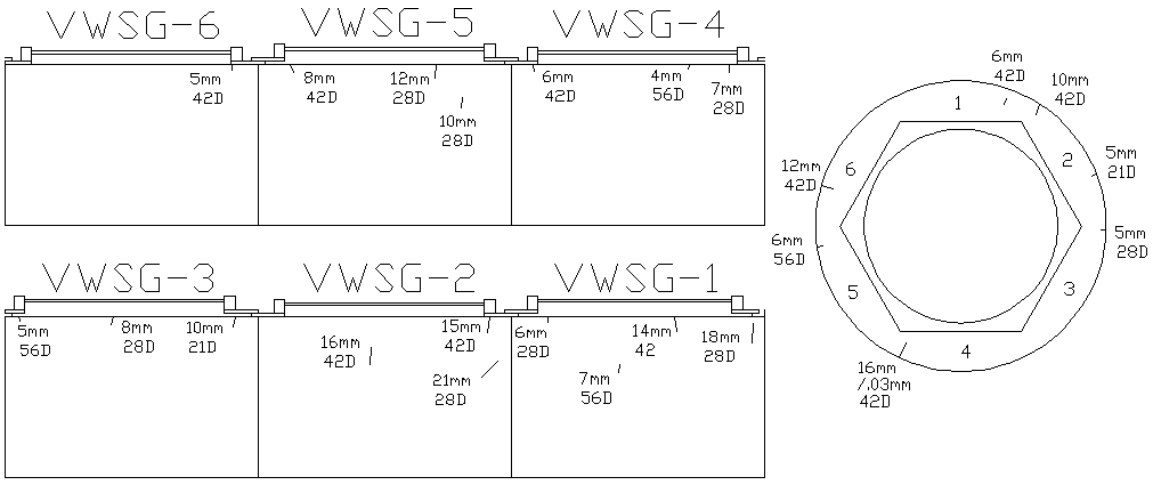

Figure 4.31 Crack Map of G1-HPC-FA

Table 4.15 below presents the crack growth behavior of the Group 2 mixes, by comparing the number of cracks at various ages. Compared to the Group 1 mixes, the Group 2 mixes each had a greater number of cracks. This is likely due to the increased hydration rate of the HES-HPC mixes.

Table 4.15 Crack Growth in Group 2 Mixes

Age	Number of Cracks			
	G2-HES-SL		G2-HES-FA	
	Normal Curing	Heat Blanket Curing	Normal Curing	Heat Blanket Curing
21	6	2	10	8
28	10	15	12	17
42	16	19	13	13
56	7	11	8	8
Total	39	47	43	46
Observed Cracking Age	**28**	**28**	**35**	**Did Not Crack**

The crack maps for the normally cured and heat blanket cured G2-HES-SL are presented in Figure 4.32 and Figure 4.33, respectively. Based on the number of cracks, the ring cured under the heat blanket appears to experience more severe cracking, with 20.5% more cracks by the 56 day testing period. However, the heat cured ring does not experience a crack that propagates from the edge of the concrete to the steel, which is shown in the normally cured ring. The heat blanket cured ring does experience cracking at the steel, which is also recognized in the FSG. The cracking day of the normally cured ring, as specified by AASHTO PP34, is day 28. Although a crack did not propagate from the edge of the concrete to the steel, the cracking day for the heat cured sample is also recorded as day 28, because the FSG saw a jump in the strain reading at the time a crack formed at the steel. Despite the differences in total number of cracks and crack growth rates, both rings had the same cracking age, as specified by AASHTO PP34.

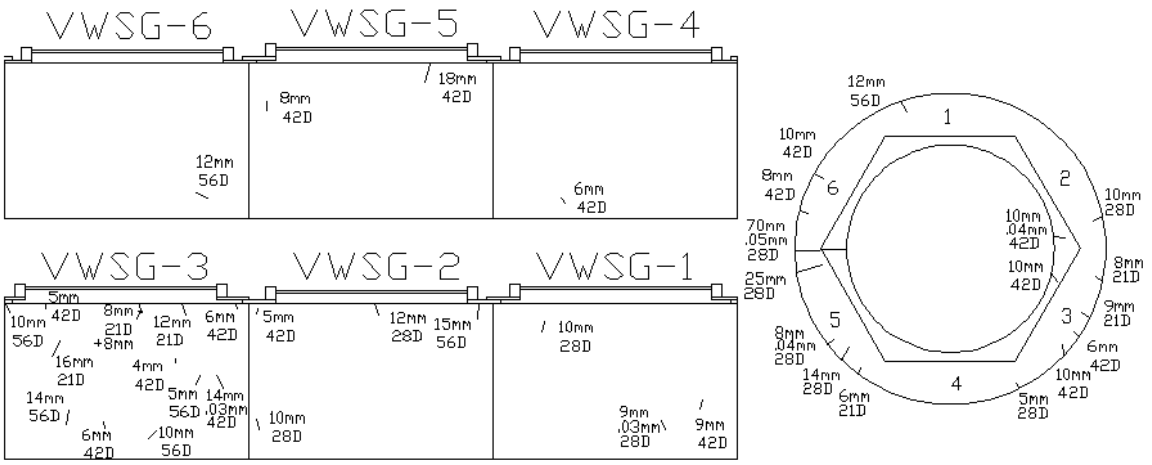

Figure 4.32 Crack Map of G2-HES-SL – Normal Curing

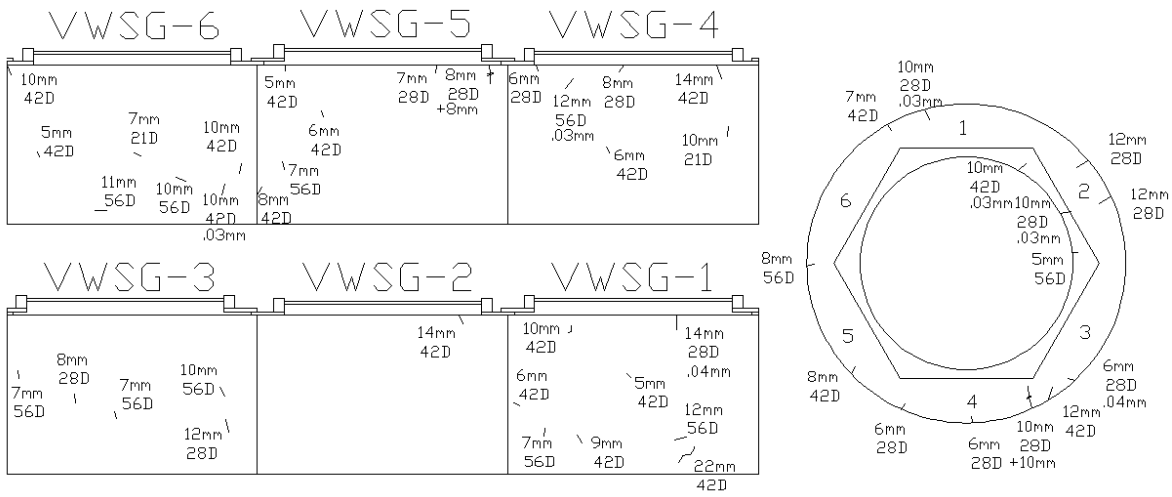

Figure 4.33 Crack Map of G2-HES-SL – Heat-Blanket Curing

The crack map for the normally cured and heat blanket cured G2-HES-FA are presented in Figure 4.34 and Figure 4.35, respectively. Unlike the Slag mix, the Flyash mix only showed a 7.0% increase in total number of cracks when heat blanket curing was applied. For comparison, the free drying shrinkage increased by 7.8% when heat blanket curing was applied. The normal cured ring cracked at approximately day 35, while the heat blanket cured ring did not crack during the 56 day testing period. The crack in the normally cured ring was accurately located by the VWSGs. The heat cured ring showed a

high concentration of cracks near VWSG-4 and VWSG-5, which showed the highest tensile strain readings of the VWSGs. Overall the Flyash mix showed a slight increase in cracking compared to the Slag mix.

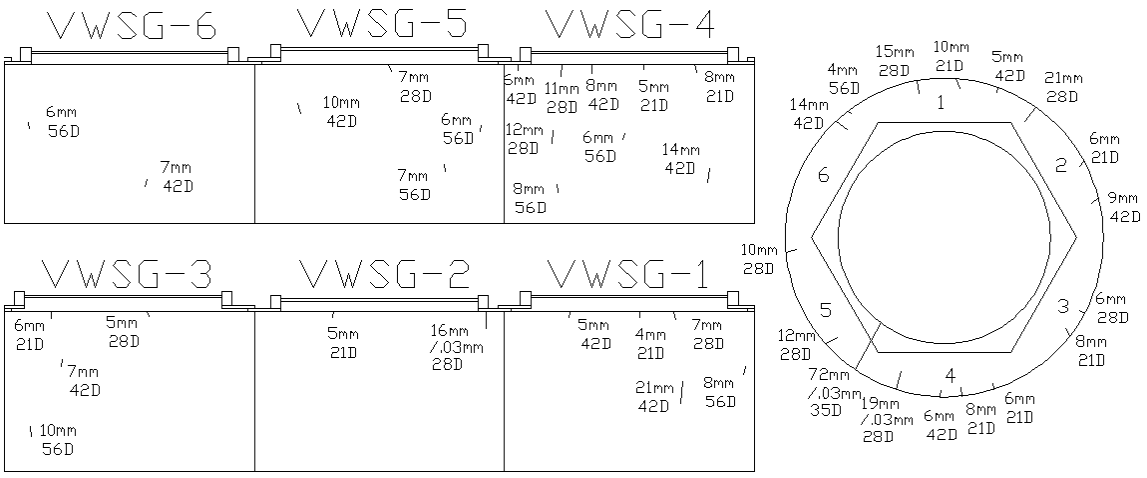

Figure 4.34 Crack Map of G2-HES-FA – Normal Curing

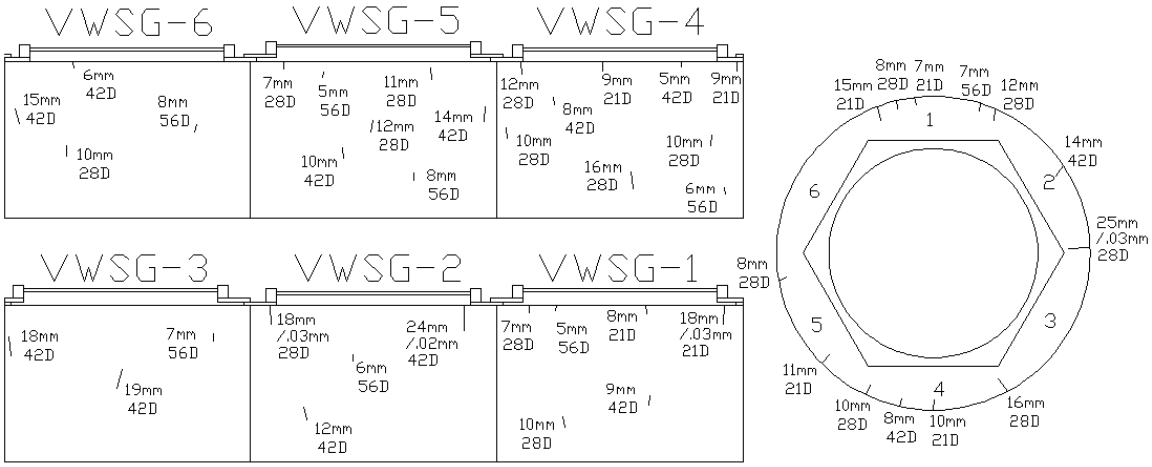

Figure 4.35 Crack Map of G2-HES-FA – Heat-Blanket Curing

Table 4.16 below presents the crack growth behavior of the Group 3 mixes, by comparing the number of cracks at various ages. Based on the table, adding SRA to the Slag mix lead to a nearly identical crack development for both curing methods. For the G3-SRA-FA, the difference between the crack developments of normal and heat-blanket curing is minimal. A crack fully penetrating through the top of the normally cured G3-SRA-FA occurred on day 39. However, the strain gages did not indicate any cracking at this location on the ring and occurred at the same location as one of the bolts. This is likely due to increased stress at the location of the bolt, and was not suspected to be a restrained shrinkage crack. Crack development appears to correlate well with the free drying shrinkage results, where the mixes with higher free drying shrinkage also had an increase in the number of cracks. Additionally, SRA had a less significant effect on reducing the number of cracks for the Flyash based mixes; a 7.0% and 8.7% decrease for normal and heat blanket curing, respectively.

Table 4.16 Crack Growth in Group 2 Mixes

Age	Number of Cracks			
	G3-SRA-SL		G3-SRA-FA	
	Normal Curing	Heat Blanket Curing	Normal Curing	Heat Blanket Curing
21	9	9	8	12
28	14	12	15	13
42	9	13	13	16
56	3	1	4	1
Total	35	35	40	42
Observed Cracking Age	**Did Not Crack**	**Did Not Crack**	**39***	**Did Not Crack**

***Strain gages did not indicate any crack forming**

The crack maps for the normally cured and heat blanket cured G3-SRA-SL are presented in Figure 4.36 and Figure 4.37, respectively. Compared to the normally cured G2-HES-SL, the normally cured G3-SRA-SL saw a 10.3% decrease in total cracks formed. Compared to the heat-blanket cured G2-HES-SL, the heat-blanket cured G3-SRA-SL saw a 35.2% decrease in total cracks formed. Furthermore, neither ring from the G3-SRA-SL mix cracked, while its HES counterpart cracked for both normal and heat curing. Comparing the normal and heat-blanket cured rings, there did not appear to be any difference in the crack development, with both developing the same number of cracks and neither developing a significant crack. The benefits for SRA showed for both curing conditions, but SRA had a much greater effect when heat-blanket curing was used.

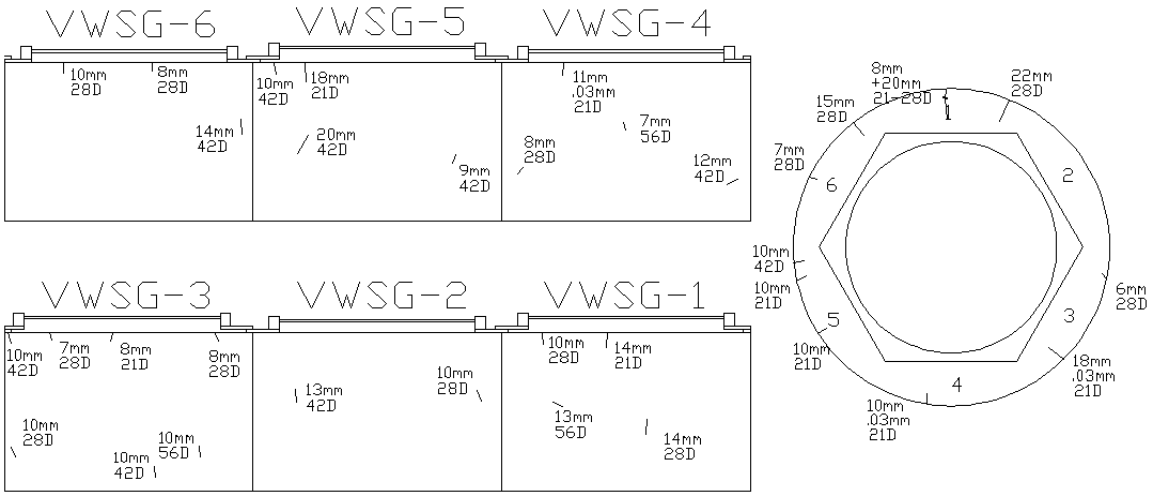

Figure 4.36 Crack Map of G3-SRA-SL – Normal Curing

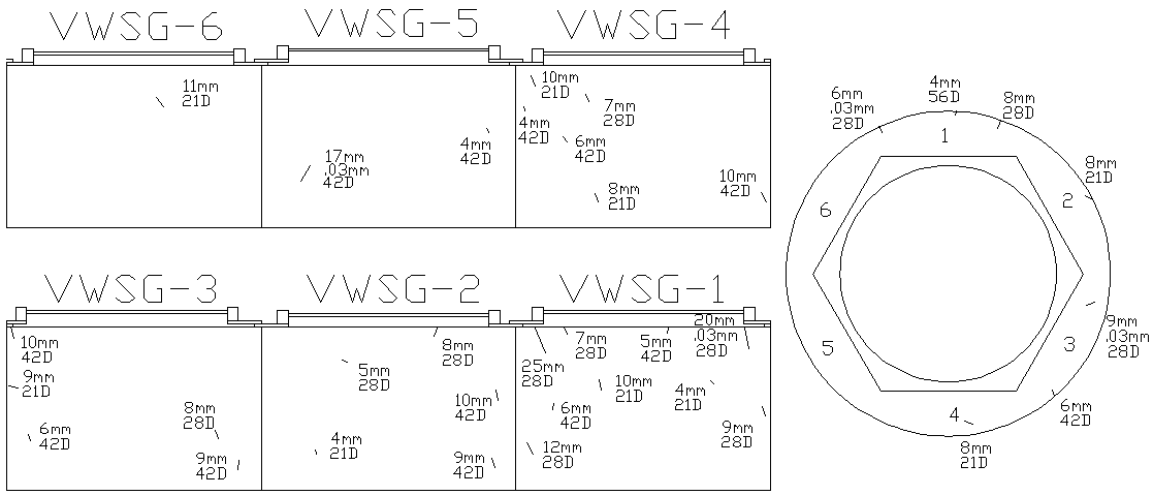

Figure 4.37 Crack Map of G3-SRA-SL – Heat-Blanket Curing

The crack maps for the normally cured and heat blanket cured G3-SRA-FA are presented in Figure 4.38 and Figure 4.39, respectively. The SRA did not appear to have a significant effect on reducing total number of cracks for the mixes containing Flyash. This agrees with the free shrinkage results, which did not witness a significant decrease in free shrinkage strain. The results do show a similar trend to the G3-SRA-SL mixes, which shows similar crack development patterns for both normal and heat-blanket curing. The normally cured ring did show a crack penetrating throughout the thickness of the concrete along the top of the ring, while the heat cured ring did not. Since the crack occurred along the bolt of the embedded VWSGs, it is believed this may be the cause for this result. Neither the VWSGs nor FSGs indicated a crack, further leading one to believe the added stress around the bolt caused the cracking. Still the crack was recorded as being initially formed around day 28 but did not propagated fully to the steel until day 39.

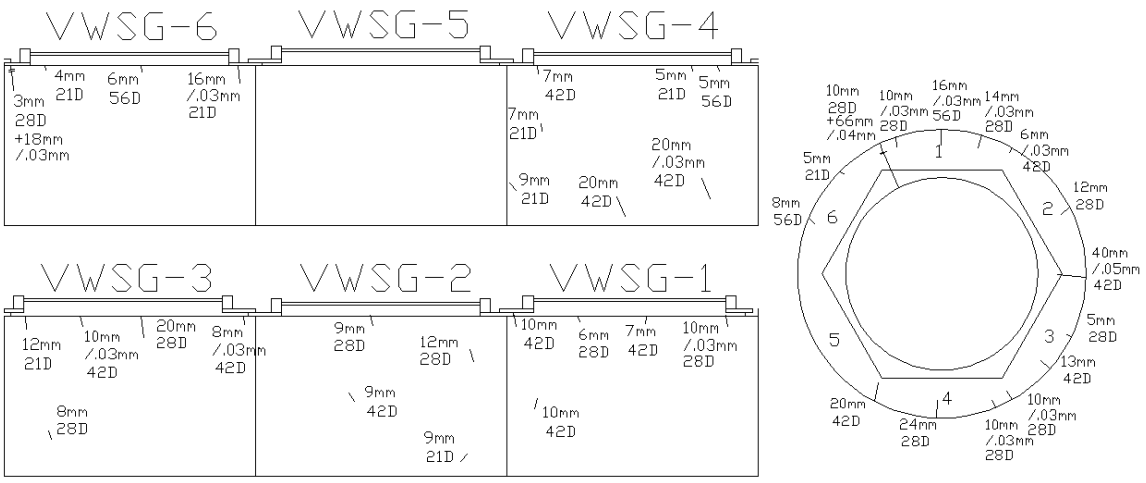

Figure 4.38 Crack Map of G3-SRA-FA – Normal Curing

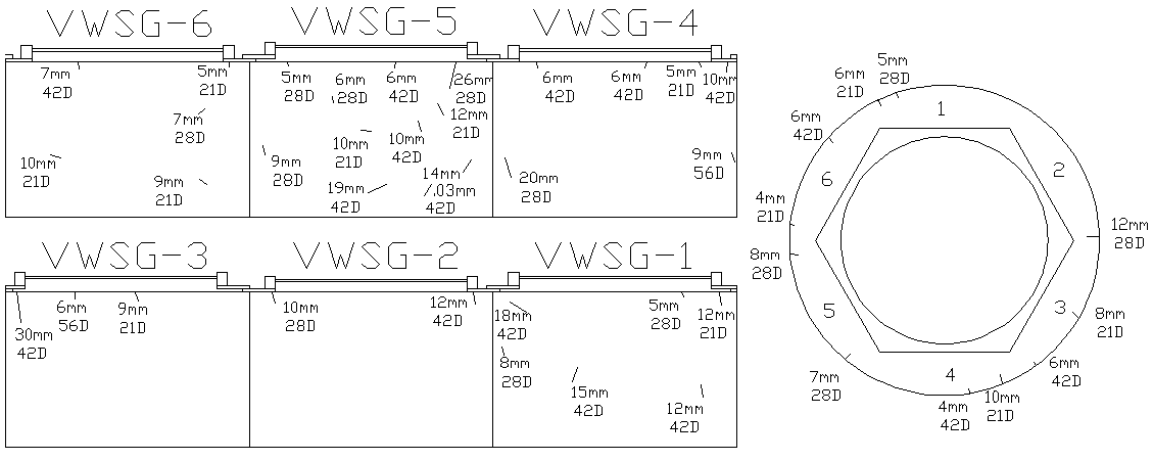

Figure 4.39 Crack Map of G3-SRA-FA – Heat-Blanket Curing

4.4.4 Correlation between Free Shrinkage and Restrained Shrinkage

The relationship between free and restrained shrinkage is evaluated below. It is important to note that the restrained shrinkage test largely depends on the geometry of the concrete and geometry of the steel. Differences in these geometries are related to the degree of restraint. Still, the free shrinkage results can be a good indicator of the restrained shrinkage test results. Also, it is important to note the restrained shrinkage test

is best used for comparing several mixes and not for determining the cracking potential of a single mix.

Aktas (2007) and Ates (2010) plotted the strain in concrete from the restrained shrinkage test vs. the free shrinkage strain. They found the slope of the linear trend line to correlate with the cracking potential. They both agreed that a larger value for the slope correlated with a greater likelihood of cracking. Aktas reported slopes larger than 0.4 lead to early cracking, slopes lower than 0.2 lead to no cracking, and everything in between lead to later age cracking or no cracking, but with high tensile strains. Despite these results, it is not mentioned how a mix with low free and restrained shrinkage will not crack while still being able to have a large slope.

Figure 4.40 shows the free and restrained shrinkage correlation for the Group 2 mixes. As shown by the trend lines, the normally cured G2-HES-SL has a slope more than twice as large as the heat-blanket cured ring. Both rings cracked on the same day, and the heat cured ring contained a higher number of total cracks. Similarly, the trend line for the normally cured G2-HES-FA has a slope more than twice as large as the heat-blanket cured ring, despite having a similar cracking trend. This is one example of the slope of the trend lines not correlating well with the results of the restrained shrinkage test. In addition, the Group 2 mixes contained larger free and restrained shrinkage values than the Group 3 mixes, which showed much less cracking due to the inclusion of SRA.

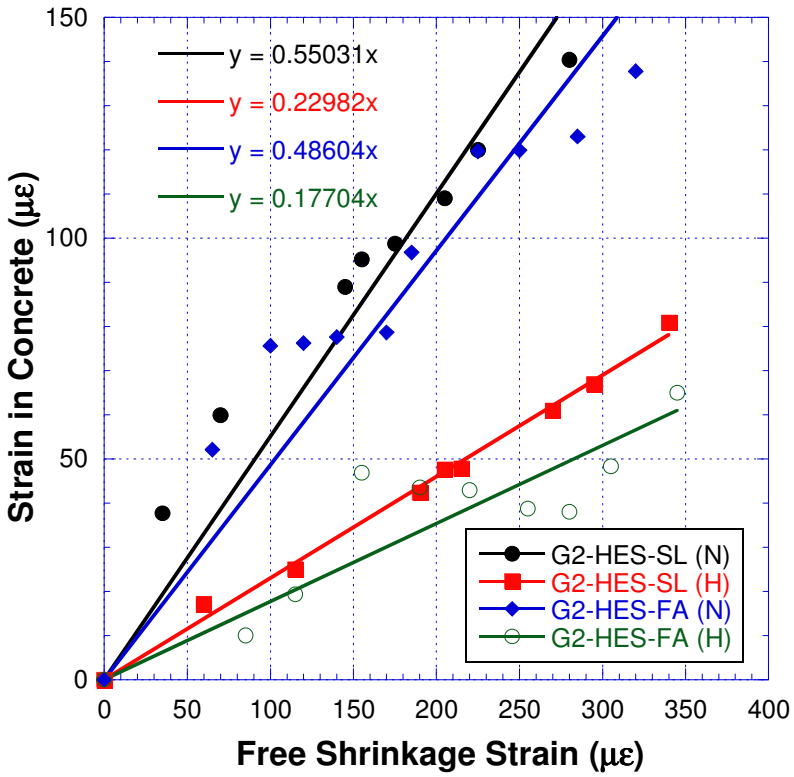

Figure 4.40 Free and Restrained Shrinkage Correlation – Group 2 Mixes

Figure 4.41 shows the free and restrained shrinkage correlation for the Group 3 mixes. As seen in the trend lines, the mixes containing SRA had both a lower free shrinkage strain and a lower restrained shrinkage strain by 56 days. Despite this, the slope for the normally cured G3-SRA-SL ring was over 0.5 yet experienced the least number of cracks and did not have a restrained shrinkage crack. This slope is also much larger than that of the heat cured sample from the same mix, despite having a nearly identical crack development, as shown by the crack maps. The normally cured G3-SRA-FA ring did show a crack despite a lower slope value, although this crack may be due to the concrete being weaker near the bolt.

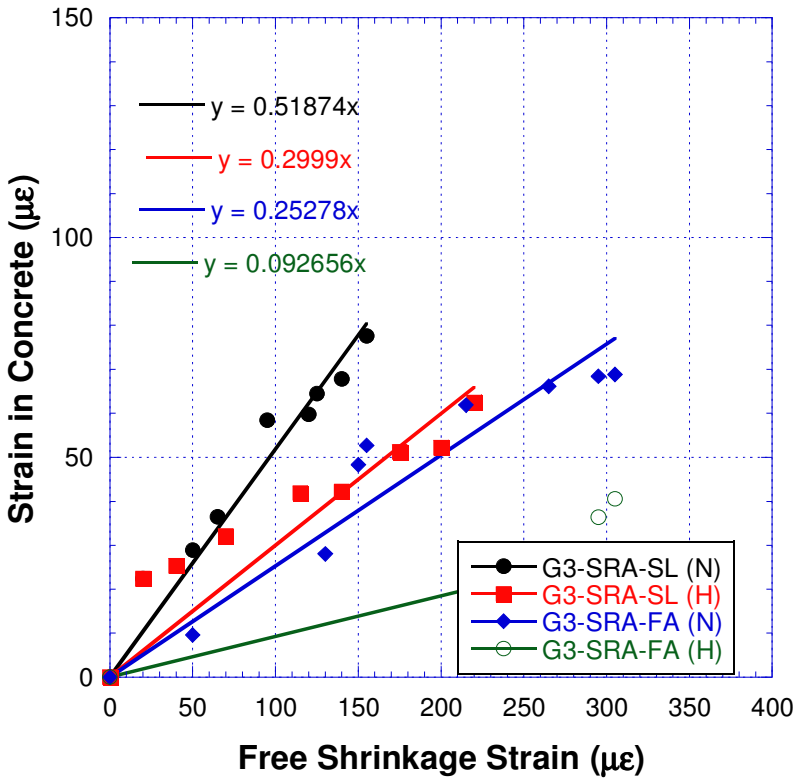

Figure 4.41 Free and Restrained Shrinkage Correlation – Group 3 Mixes

Despite what the previous studies have shown, the value of slope did not correlate well with how the mix performed in the ring test. In general, most slopes did appear to be between 0.2 and 0.5. It can be inferred that mixes with a result outside of this range, for the given ring geometries, may need to be repeated, as there should be correlation to some degree between free and restrained shrinkage. Results outside this range may indicate improper curing, poor consolidation or errors in testing as the reasons for the unexpected correlation. This is just a theory that will need many more tests to confirm and could be the focus of a future study.

4.4.5 Correlation between FSGs and VWSGs

Based on the study performed by Hossain and Weiss (2004), it is suggested the stress in the steel and concrete can be estimated just by knowing the ring geometries and the results of the FSG readings. As previously stated, the equation used for their study is as follows:

$$\sigma_{Actual-Max}(t) = \varepsilon_{Steel}(t) * E_S * C_{1R} * C_{2R}$$

Where C_{1R} and C_{2R} are constants related to the geometries and properties of the steel and concrete. This equation is used to calculate the "actual residual stress" by accounting for any stress relaxation. However, this equation assumes that the radial displacement on the steel is uniform. This is the ideal scenario the ring test tries to accomplish, but the reason the restrained shrinkage test has shown high variability is because this is not the actual scenario for the ring test. Furthermore, the authors did not monitor the concrete strains in the ring test so there is no confirmation if the stress in the steel matches the stress in the concrete. Based on the VWSG results, there is a much more complicated development of strain in the concrete and is not uniform as the above study suggested. The following section relates the stress determined by the equation above, and the stress calculated from the VWSGs and results of the elastic modulus test.

Table 4.17 contains the results of the calculated (expected) maximum tensile stress from the equation presented by Weiss and the actual maximum tensile stress calculated from the VWSG strain readings and results of the modulus of elasticity test. The table also includes the corresponding strain values for comparison with the cracking strain. For most of the rings, the expected tensile stress shows a fairly significant difference from the actual tensile stress. This can be explained by a non-uniform stress

distribution in the rings. It is important to note a significant crack appeared in the normally cured G2-HES-SL and appeared to have a large tensile stress development based on the VWSGs. This is due to the setup of the VWSGs, which are embedded along the top of the ring. As a severe crack develops, the stress in the steel ring will be released and will be read properly by the FSGs. However, the VWSGs will continue to expand due to the split in the concrete increase the distance between the embedment points in the concrete. Prior to cracking, the VWSGs monitor the strain in the concrete along six sides of the ring, and accurately signals the location of cracking. The equation presented by Weiss is an ideal case which does not consistently correlate well with the actual stresses in the concrete, as shown by the VWSGs.

Table 4.17 Comparison of Expected Concrete Stress-Strain to Actual Concrete Stress-Strain

Tensile Stress (psi)	G2-HES-SL		G2-HES-FA		G3-SRA-SL		G3-SRA-FA	
	Normal	Heat	Normal	Heat	Normal	Heat	Normal	Heat
Expected (FSGs)	**361***	507	**477***	477	275	383	477	563
Actual (VWSGs)	**674***	500	**759***	401	343	379	408	354
% Difference	**60.4%***	1.4%	**45.6%***	17.3%	22.0%	1.1%	15.6%	45.6%
Strain (με)	G2-HES-SL		G2-HES-FA		G3-SRA-SL		G3-SRA-FA	
	Normal	Heat	Normal	Heat	Normal	Heat	Normal	Heat
FSG	60	84	83	79	46	64	79	93
VWSG	105	81	119	37	57	63	77	67
Cracking Strain	102 (Crack)	100	120 (crack)	107	128	115	118	113

***Stress calculated at time of cracking**

4.5 REVIEW OF SRA'S AND HEAT CURING'S EFFECTS ON EARLY AGE STRENGTH AND ULTIMATE DRYING SHRINKAGE

It is important to review the previous discussions of how SRA affects early age strength gain and the ultimate drying shrinkage to determine its applicability in HES-HPC mix designs. As previously stated, adding SRA to the mixes lead to a decrease in early age strength and a decrease in ultimate drying shrinkage. However, it must be determined if the solution to minimizing shrinkage while still maintaining a high early age strength should be to adjust the curing temperature or to adjust the SRA dosage.

Table 4.17 includes the percent of strength and free shrinkage decrease at each age due to SRA, while Table 4.18 includes the percent of strength and free shrinkage decrease due to not using heat-blanket curing. As can be seen in Table 4.17, SRA has a much greater effect on shrinkage than early age strength for the Slag based mixes. The percent change in free shrinkage was nearly twice as large as the change in the 6 hour strength. It is not known why this is not also shown in the Flyash mixes. Also, by the 24 hour test, the effects become insignificant. As can be seen by Table 4.18, temperature had a very significant effect on strength, but not on the ultimate free drying shrinkage. The 6 and 8 hour strengths decrease by 73%-84% when not using the heat blanket, while the ultimate free drying shrinkage decreases by 16%-26%, approximately 3-5 times as much of an effect. These results show that early age curing temperature has a more significant effect on temperature, while SRA has a more significant effect on the ultimate free drying shrinkage. Additionally, both have only minor effects on the 28 day compressive strength.

Table 4.18 Compressive Strength and 91 Day Free Drying Shrinkage Loss Due to SRA

Compressive Strength Loss (%)				
Age	G2-HES-SL – G3-SRA-SL		G2-HES-FA – G3-SRA-FA	
	Normal	1 day heat	Normal	1 day heat
6 hr	25.4%	23.5%	43.0%	38.2%
8 hr	27.1%	14.1%	44.0%	12.3%
12 hr	17.2%	10.4%	29.4%	13.1%
24 hr	11.1%	10.9%	10.1%	2.1%
3 day	10.2%	13.4%	2.3%	-0.5%
14 day	14.7%	7.6%	12.9%	10.9%
28 day	-7.9%	-1.9%	9.4%	11.2%
Decrease in 91 day Free Drying Shrinkage (%)				
Age	G2-HES-SL – G3-SRA-SL		G2-HES-FA – G3-SRA-FA	
	Normal	1 day heat	Normal	1 day heat
91 day	49.2%	42.3%	25.7%	17.5%

Table 4.19 Compressive Strength and 91 Day Free Drying Shrinkage Loss When Heat Blanket Curing Was Not Used

Compressive Strength Loss (%)				
Age	G2-HES-SL	G2-HES-FA	G3-SRA-SL	G3-SRA-FA
6 hr	76.0%	83.0%	76.6%	84.3%
8 hr	73.6%	73.5%	77.6%	83.1%
12 hr	39.2%	36.6%	43.8%	48.5%
24 hr	25.3%	15.6%	25.5%	22.5%
3 day	10.4%	4.4%	7.1%	7.0%
14 day	-7.6%	-1.8%	0.7%	0.5%
28 day	-1.5%	-2.0%	-7.5%	-4.1%
Decrease in 91 day Free Drying Shrinkage (%)				
Age	G2-HES-SL	G2-HES-FA	G3-SRA-SL	G2-SRA-FA
91 day	16.7%	7.5%	26.7%	16.7%

CHAPTER 5

SUMMARY AND CONCLUSIONS

5.1 SUMMARY AND CONCLUSIONS

The purpose of this study was to monitor how heat-blanket curing effects early age strength gain, and free and restrained shrinkage. AASHTO PP34 was modified to include VWSGs embedded in the concrete, in order to correlate the results with the FSGs. Additionally, further steps were taken to determine the applicability of using SRA in HES-HPC. Six mix designs were used to monitor the differences between HPC and HES-HPC, as well as the differences between normal and heat-blanket curing. Due to the high sensitivity of concrete during the first 24 hours after pouring, each mix was performed three times in order to show this sensitivity by reporting the variation in early age compressive strength. Free shrinkage and ring samples were cured under wet burlap for 14 days for normal curing. For heat-blanket curing they were covered with wet burlap and placed in an insulated chamber under a heat blanket with a constant temperature of 120°F for 24 hours, followed normal wet burlap curing until day 14.

Based on the results of this study, the following conclusions were made:

1) SRA has a much more significant effect on reducing ultimate free drying shrinkage than it does on reducing 6 hour compressive strength. High temperature during curing has a much more significant effect on early age strength gain than it does on increasing shrinkage. This implies that a

combination of higher curing temperature and an appropriate dosage of SRA can be used in conjunction to develop HES concrete with lower shrinkage strains.

2) Higher curing temperature resulted in lower 28 day compressive strength, but not significantly (within 10%). Including SRA in the mixes resulted in a negligible difference in 28 day compressive strength. Both of these results are commonly supported by many researchers.

3) Despite the results of the studies performed by Aktas (2007) and Ates (2010), the trend lines developed from plotting the free and restrained shrinkage together does not accurately predict the likelihood of cracking. Low values for both free and restrained shrinkage can still show larger slope in the trend line, yet show a much better performance in resisting cracking. This was proved by the results from the free and restrained shrinkage tests for the mixes containing SRA. However, the slope of the trend line could implicate some error in testing, as free and restrained shrinkage should correlate to some degree.

4) VWSGs can accurately signal the timing and location of cracking better than the FSGs. The VWSGs show a complicated stress distribution that is not indicated by the FSGs. However, the VWSGs in the setup used for this experiment continued to show an increase in tensile strain after cracking.

5) Although the maximum stress can be estimated by the equation presented by Hossain and Weiss (2004), it does not always correlate well with the actual stress/strain in the concrete as shown by the VWSGs. This is likely due to an

uneven stress distribution in the ring. The restrained shrinkage test, as well as the equation presented by Hossain and Weiss, assumes an even stress distribution.

5.2 SCOPE FOR FUTURE RESEARCH

The experimental program performed in this study can be expanded upon to cover a wider range of curing temperatures and SRA dosages. Altering the mix designs presented in this paper can help one develop a more durable HES-HPC. Because of the high variability of the restrained shrinkage ring test, many mixes with multiple rings can help to further confirm the conclusions presented by this report. Further study is required to determine how HES-HPC performs in the field. Another experimental program can determine how the live load in adjacent lanes will affect early age concrete. In addition, the VWSG setup used in this study can be examined to determine if there are more accurate methods for monitoring the strain in the concrete. Additionally, a study can be done to correlate the results of the AASHTO ring test and the ASTM ring test. The different concrete and steel geometries of each standardized test method relates to different degrees of restraint. Correlating the two test methods will allow for a better comparison between studies despite differences in the ring geometry.

REFERENCES

1. Emborg, M., Bernander, S., "Assessment of Risk of Thermal Cracking in Hardening Concrete", Journal of Structural Engineering, Vol. 120, No. 10, 1994, pp 2893-2912.
2. Acker, P., Ulm, F., "Creep and Shrinkage of Concrete: Physical Origins and Practical measurements", Nuclear Engineering and Design, Vol. 203, 2001, pp 143-158.
3. Schutter, G. D., "Finite Element Simulation of Thermal Cracking in Massive Hardening Concrete Elements Using Degree of Hydration Based Material Laws", Computers and Structures, Vol. 80, 2002, pp 2035-2042.
4. Tia, M., Subramanian, R., Brown, D., Broward, C., "Evaluation of Shrinkage Cracking Potential of Concrete Used in Bridge Decks in Florida", Report No. BC-354, September 2005.
5. Lura, P., Pease, B., Mazzotta, G., Rajabipour, F., Weiss, J., "Influence of Shrinkage-Reducing Admixtures on the Development of Plastic Shrinkage Cracks", ACI Materials Journal, Vol. 104, No. 2, March 2007, pp 187-194.
6. Bents, D. P., Geiker, M. R., Hansen, K. K., "Shrinkage-Reducing Admixtures and Early-Age Desiccation in Cement Pastes and Mortars", Cement and Concrete Research, Vol. 31, No. 7, July 2001, pp 1075-1085.
7. Nassif, H., Suksawang, N., "Effect of Curing Methods on Durability of High-Performance Concrete", Transportation Research Record, Vol. 1798, 2002.
8. Nassif, H., Najm, H., Aktas, K., "Concrete Shrinkage Analysis for Bridge Deck Concrete", Report No. FHWA NJ-2007-007, December 2007.

9. Loser, R., Leemann, A., “Shrinkage and Restrained Shrinkage Cracking of Self-Compacting Concrete Compared to Conventionally Vibrated Concrete”, Materials and Structures, Vol. 42, 2009, pp 71-82.
10. ASTM C 1581/C 1581M – 09a, “Standard Test Method for Determining Age at Cracking and Induced Tensile Stress Characteristics of Mortar and Concrete under Restrained Shrinkage”.
11. Lee, K. M., Lee, H. K., Lee, S. H., Kim, G. Y., “Autogenous Shrinkage of Concrete Containing Granulated Blast-Furnace Slag”, Cement and Concrete Research, Vol. 36, 2006, pp 1279-1285.
12. Lee, H. K., Lee, K. M., Kim, Y. H., Yim, H., Bae, D. B., “Ultrasonic In-Situ Monitoring of Setting Process of High-Performance Concrete”, Cement and Concrete Research, Vol. 34, 2004, pp 631-640.
13. Carlson, R. W., Reading, T. J., “Model Study of Shrinkage Cracking in Concrete Building Walls”, ACI Structural Journal, Vol. 85, August 1988, pp 395-404.
14. Foliard, K. J., Berke, N. S., “Properties of High-Performance Concrete Containing Shrinkage-Reducing Admixture”, Cement and Concrete Research, Vol. 27, No. 9, September 1997, pp 1357-1364.
15. Banthia, N., Azzabi, M., Pigeon, M., “Restrained Shrinkage Cracking in Fibre-Reinforced Cementitious Composites”, Materials and Structures, Vol. 26, 1993, pp 405-413.
16. Li, Z., Qi, M., Li, Z., Ma, B. “Crack Width of High-Performance Concrete due to Restrained Shrinkage”, Journal of Materials in Civil Engineering, Vol. 11, No. 3, August 1999.

17. Hossain, A. B., Pease, B., Weiss, J., “Quantifying Early-Age Stress Development and Cracking in Low Water-to-Cement Concrete: Restrained-Ring Test with Acoustic Emission”, Transportation Research Record, Vol. 1834, 2003.
18. Byard, B. E., Schindler, A. K., Barnes, R. W., Rao, A., “Cracking Tendency of Bridge Deck Concrete”, Transportation Research Record, 2010, pp 122-131.
19. Hossain, A. B., Weiss, J., “Assessing Residual Stress Development and Stress Relaxation in Restrained Concrete Ring Specimens”, Vol. 26, No. 5, July 2004, pp 531-540.
20. Atis, C. D., “High-Volume Fly Ash Concrete with High Strength and Low Drying Shrinkage”, Journal of Materials in Civil Engineering, Vol. 15, No. 2, April 2003.
21. Kayali, O., Haque, M. N., Zhu, M. N., “Drying of Fibre-Reinforced Lightweight Aggregate Concrete Containing Fly Ash”, Cement and Concrete Research, Vol. 29, No. 11, November 1999, pp 1835-1840.
22. Termkahjornkit, P., Nawa, T., Nakai, M., Saito, T., “Effect of Fly Ash on Autogenous Shrinkage”, Cement and Concrete Research, Vol. 35, No. 3, March 2005, pp 473-482.
23. Mazloom, M., Ramezanianpour, A. A., Brooks, J. J., “Effect of Silica Fume on Mechanical Properties of High-Strength Concrete”, Cement and Concrete Composites, Vol. 26, No. 4, May 2004, pp 347-357.
24. Li, J., Yao, Y., “A Study on Creep and Drying Shrinkage of High Performance Concrete”, Cement and Concrete Research, Vol. 31, No. 8, August 2001, pp 1203-1206.

25. Haque, M. N., “Strength Development and Drying Shrinkage of High-Strength Concretes”, Cement and Concrete Composites, Vol. 18, No. 5, 1996, pp 333-342.
26. Aktas, K., “Assessment of Cracking Potential of High-Performance Concrete due to Restrained Shrinkage”, M.S. Thesis, Rutgers University, 2007.
27. Ates, U., “Effect of Pozzolanc Material on the Restrained Shrinkage Behavior of Self-Consolidating Concrete”, M.S. Thesis, Rutgers University, 2010.
28. Kovler, K., Zhutovsky, S., “Overview and Future Trends of Shrinkage Research”, Materials and Structures, Vol. 39, No. 9, 2006, pp 827-847.
29. Huo, X. S., Wong, L. U., “Experimental study of early-age behavior of high performance concrete deck slabs under different curing methods”, Construction and Building Materials, Vol. 20, 2006, pp 1049-1056.
30. Nassif, H., Najm, H., Suksawang, N., “Effect of pozzolanic materials and curing methods on the elastic modulus of HPC”, Cement and Concrete Composites, Vol. 27, 2005, pp 661-670.
31. Kim, J. K., Moon, Y. H., Eo, S. H., “Compressive Strength Development of Concrete with Different Curing Time and Temperature”, Cement and Concrete Research, Vol. 28, No. 12, 1998, pp 1761-1773.

APPENDIX A

RESTRAINED SHRINKAGE – EXPECTED AND ACTUAL TENSILE STRESS

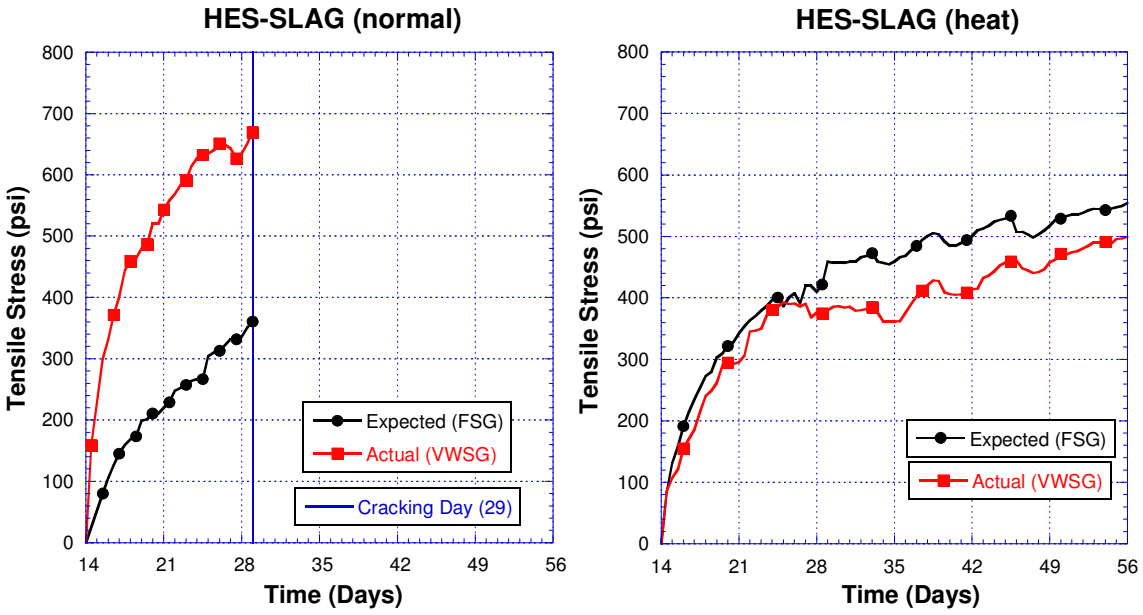

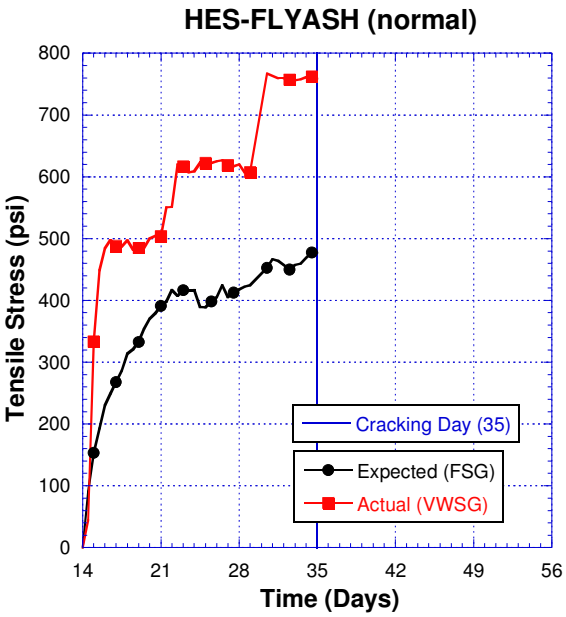
HES-FLYASH (normal)
Tensile Stress (psi)
Time (Days)
Cracking Day (35)
Expected (FSG)
Actual (VWSG)

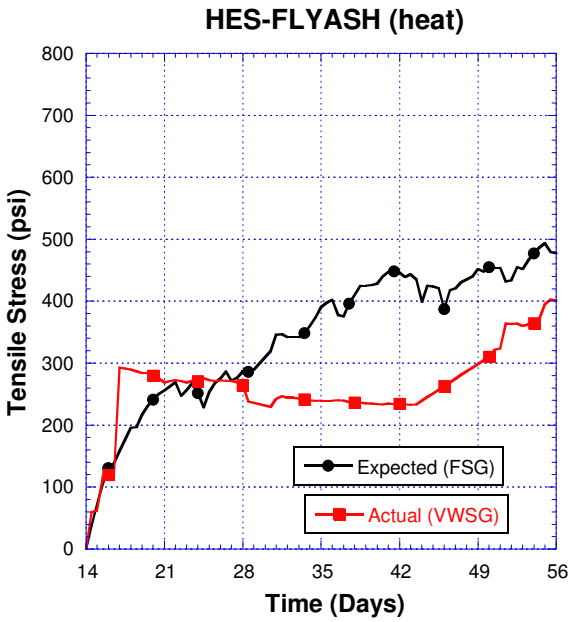
HES-FLYASH (heat)
Tensile Stress (psi)
Time (Days)
Expected (FSG)
Actual (VWSG)

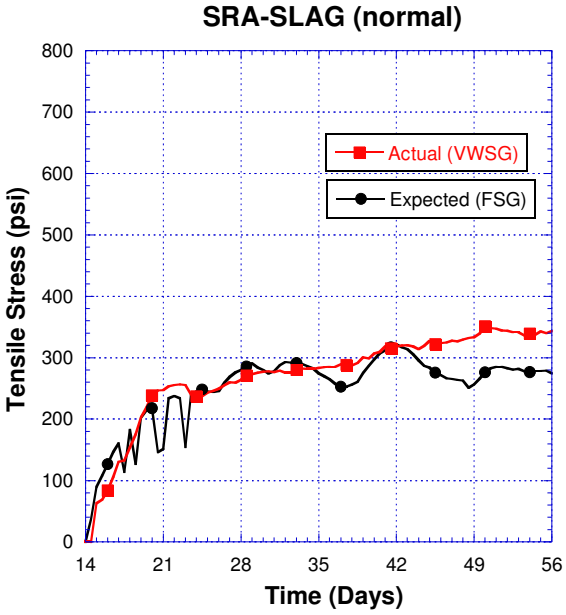
SRA-SLAG (normal)
Tensile Stress (psi)
Time (Days)
Actual (VWSG)
Expected (FSG)

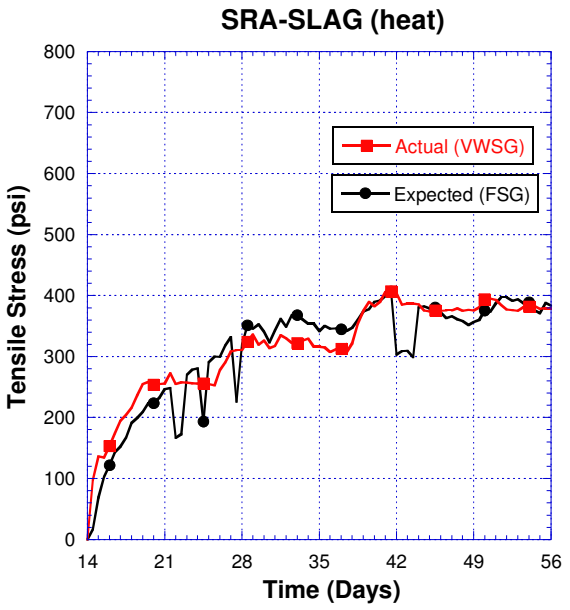
SRA-SLAG (heat)
Tensile Stress (psi)
Time (Days)
Actual (VWSG)
Expected (FSG)

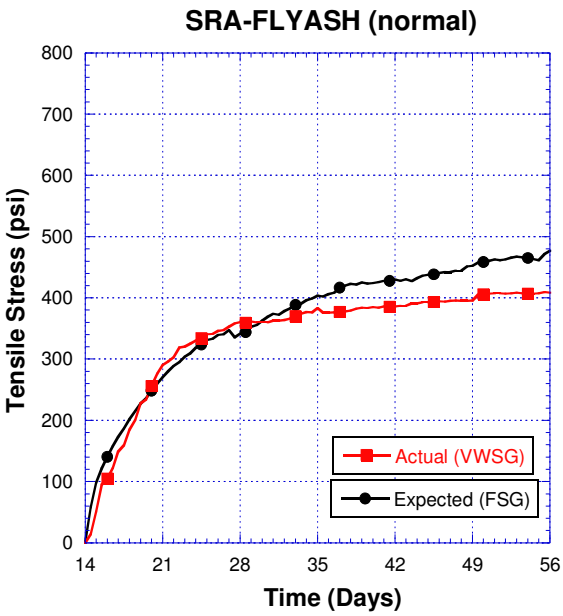
SRA-FLYASH (normal)
Tensile Stress (psi)
800
700
600
500
400
300
200
100
0
14
21
28
35
42
49
56
Time (Days)
Actual (VWSG)
Expected (FSG)

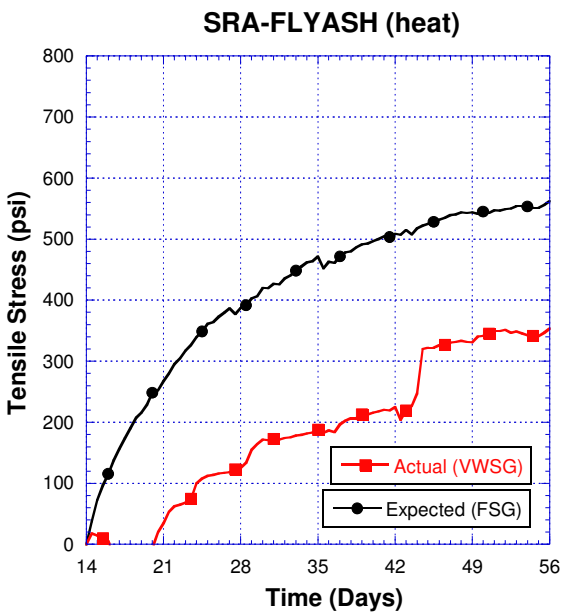
SRA-FLYASH (heat)
Tensile Stress (psi)
800
700
600
500
400
300
200
100
0
14
21
28
35
42
49
56
Time (Days)
Actual (VWSG)
Expected (FSG)